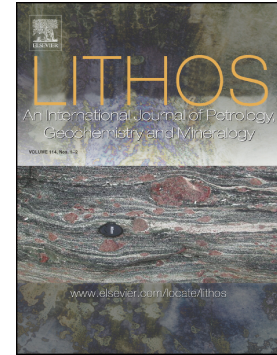# Journal Pre-proof

Experimental and thermodynamic constraints on mineral equilibrium in pantelleritic magmas

Pierangelo Romano, Bruno Scaillet, John C. White, Joan Andújar,
Ida Di Carlo, Silvio G. Rotolo

Please cite this article as: P. Romano, B. Scaillet, J.C. White, et al., Experimental and thermodynamic constraints on mineral equilibrium in pantelleritic magmas, *LITHOS* (2020), https://doi.org/10.1016/j.lithos.2020.105793

Experimental and thermodynamic constraints on mineral equilibrium in pantelleritic magmas

Pierangelo Romano[1,*] pierangeloromano@gmail.com, Bruno Scaillet[2], John C. White[3], Joan Andújar[2], Ida Di Carlo[2], Silvio G. Rotolo[1,4]

[1]Dipartimento di Scienze della Terra e del Mare (DiSTeM), Università degli Studi di Palermo, Via Archirafi 22, 90123 Palermo, Italy

[2]Institut des Sciences de la Terre d'Orléans (ISTO) UMR 7327, Université d'Orléans – CNRS – BRGM, Campus Géosciences, 1A rue de la Férollerie, 45071 ORLÉANS Cedex 2, France

[3]Department of Geoscience, Eastern Kentucky University, Richmond, KY 40475, USA

[4] Istituto Nazionale di Geofisca e Vulcanologia, sezione di Palermo, Via Ugo la Malfa 153, 90146 Palermo, Italy

[*]Correspondig author: Pierangelo Romano, Ph.D, Dipartimento di Scienze della Terra e del Mare (DiSTeM), Università degli Studi di Palermo, Via Archirafi 22, 90123 Palermo, Italy.

1. Introduction

Peralkaline trachyte and rhyolite (peralkalinity index calculated as P.I.=[mol Na+K/Al] ≥ 1.0) frequently represent the felsic end-member in bimodal magmatic suites that characterize both oceanic and continental intra-plate and extensional tectonic settings. The origin of these magmas has been an extensively debated petrological issue, with two principal models: (i) protracted crystal fractionation from mafic (alkali gabbro) parental magma (Civetta et al., 1998; White et al., 2009; Neave et al., 2012; Romano et al., 2018), or (ii) partial melting of mafic (gabbroic) cumulates followed by low pressure crystal fractionation (e.g., Bohrson and Reid 1997; Avanzinelli et al., 2004; Macdonald et al., 2008, 2011; Marshall et al., 2009). Whatever their origin, the stability of mineral phases crystallising in peralkaline trachyte and peralkaline rhyolite (named as either

comenditic if ([Al_2O_3-4.4]/FeO* > 1.33 or pantelleritic if [Al_2O_3-4.4]/FeO* < 1.33, FeO*= total Fe as FeO; Macdonald, 1974) has been also matter of considerable discussion in the petrological community. Carmichael (1962) published the first modern detailed study of the common mineral phases occurring in pantellerite (i.e., anorthoclase, sodian clinopyroxene and amphibole, fayalitic olivine, aenigmatite) and since then there have been many studies focused on the control of temperature, pressure, oxidation and melt peralkalinity on mineral equilibrium and on how these fractionating phases, in particular feldspar and clinopyroxene, affect the transition from metaluminous (P.I. < 1.0) to peralkaline silicic magmas (e.g., Carmichael and MacKenzie, 1963; Bailey and Schairer, 1966; Nichols and Carmichael, 1969; Lindsley, 1971; Marsh, 1975; Conrad, 1984; Scaillet and Macdonald, 2001, 2003, 2006; White et al., 2005; Macdonald et al., 2011; Romano et al., 2018).

On the island of Pantelleria, the type locality for pantelleritic rocks, metaluminous trachyte and pantellerite comprise about 90% of the outcrop, occurring as ignimbrites, pumice fall deposits, or vitric lava flows and domes (Mahood and Hildreth, 1986; Jordan et al, 2018). Recent petrological modelling and experimental studies have highlighted the low temperatures (T≤ 750°C) and reducing conditions (viz., oxygen fugacities an order of magnitude or more lower than the Nickel-Nickel Oxide [NNO] buffer, or log fO$_2$ < ΔNNO-1) that characterize the pre-eruptive conditions in the pantelleritic magma chambers at Pantelleria (White et al., 2005, 2009; Di Carlo et al., 2010; Liszewska et al., 2018), and other peralkaline systems (Scaillet and Macdonald, 2001, 2003, 2006; Ren et al., 2006; White et al., 2005; Macdonald et al., 2011, 2019; Macdonald, 2012; Jeffery et al., 2017). Although considerable progress has been made, previous experimental studies have not been able to fully clarify the relationship between melt composition, intensive parameters, and the observed phenocrysts, particularly the role of fO$_2$ on mineral assemblages that indicate peralkalinity. Recent studies carried out on other (non-peralkaline) felsic systems have shown that small variations in bulk composition may profoundly affect phase relationships (and compositions), most

notably the stability fields of non-tectosilicate phases (which are minor phases in evolved silicate magmas) which are generally critical for the determination of pre-eruptive conditions (e.g., Scaillet et al., 2008; Andujar and Scaillet, 2012; Cadoux et al., 2014).

In this study we present the results of phase equilibrium experiments performed on two samples of pantellerites differing slightly in composition and mineral assemblages. Phase relationships were established at 1 kbar, for temperatures ranging between 680°C - 900°C and redox conditions around the fayalite-magnetite-quartz (FMQ) buffer (equivalent to ΔNNO-0.68 to -0.60). The experimental results are compared with the results of previous experiments carried out on similar material (Di Carlo et al., 2010). We also compare our data with thermobarometric results based on established mineral-mineral equilibria gathered from Pantelleria and other peralkaline localities (Pantelleria: White et al., 2005, 2009; Liszewska et al., 2018; Eburru, Kenya: Ren et al., 2006; and Menengai, Kenya: Macdonald et al., 2011). We focus our attention on how mineral assemblages are affected by (i) small variations of starting compositions, and (ii) temperature and redox conditions. Our findings shed new light on mineral-liquid and mineral-mineral equilibria governing the occurrence of aenigmatite, olivine, ilmenite and sodian amphibole phases in pantellerites.

2. Geological and petrological background

The island of Pantelleria is located in the Sicily Channel (Italy), within the transtensional rift system on the northern promontory of the African Plate (Figure 1). The eruptive history of Pantelleria can be subdivided into three major periods which include the formation of at least two calderas and the eruption of nine ignimbrites, each of which was followed by largely quiescent periods with occasional, volumetrically minor explosive and effusive eruptions (Jordan et al., 2018). The first period (324-190 ka) is characterized by alternating eruptions of lava flows and pumice fall deposits (Mahood and Hildreth 1986; Jordan et al., 2018). The second period (187-45 ka) begins with the formation of the La Vecchia Caldera and includes eight eruptions of trachytic to

pantellerite ignimbrite (Mahood and Hildreth 1986; Rotolo et al., 2013). The third period began

45.7 ± 1.0 ka (Scaillet et al., 2013) with the eruption of the compositionally zoned Green Tuff

(pantellerite to trachyte, Williams et al., 2014), the caldera-forming ignimbrite of the Cinque Denti

Caldera. This was followed by a prolonged period of effusive activity (to ~8 ka) that formed the

trachytic Montagna Grande-Monte Gibele shield volcano and several other pantellerite shields and

lava domes (Mahood and Hildreth, 1986; Scaillet et al., 2011). During this same period basaltic lava

flows erupted in the northwestern sector of the island (Civetta et al., 1988; Rotolo et al., 2007).

Although erupted over a long period of time and therefore clearly not belonging to the same

liquid lines of descent, peralkaline trachytes and pantellerites at Pantelleria have consistent

compositional and mineralogical trends. White et al. (2005) described five subgroups of

pantellerites, each characterized by different: (i) mineral assemblages, (ii) melt peralkalinity, and

(iii) range of temperature and fO_2. Alkali feldspar (anorthoclase) and clinopyroxene are present in

each assemblage, which differ from each other by the occurrence of oxides, fayalitic olivine, sodian

amphibole, quartz and aenigmatite minerals. Mineral assemblages with Fe-Ti oxides and fayalite

are found in rocks with the lowest P.I. (1.3-1.5) while mineral assemblages with aenigmatite ±

ilmenite are associated with P.I. > 1.5. The low temperatures of equilibration (680-720°C) together

with the reduced character (i.e., slightly below the FMQ buffer) of pantellerites have also been

experimentally constrained by Di Carlo et al. (2010) as common features of these magmas (Scaillet

et al., 2016). Melt inclusion studies have shown that despite their reduced nature, pantellerites are

also characterized by high melt water contents (H_2O_{melt} up to 4.5 wt%), along with high Cl (up 1

wt%; Lowenstern, 1994), and CO_2 usually lower than 150 ppm or barely detectable by micro infra-

red spectroscopy (Gioncada and Landi, 2010; Neave et al., 2012; Lanzo et al., 2013). Regarding the

storage pressure, field evidence suggests that peralkaline silicic magmas are stored at pressures < 2

kbar (Mahood, 1984), which has been supported at Pantelleria by thermodynamic (White et al.,

2009), experimental (Di Carlo et al., 2010), and melt inclusion (Gioncada and Landi, 2010) studies.

A low pressure of magma storage is also suggested by a phase equilibrium study of Pantelleria

trachyte (Romano et al., 2018), which also demonstrated that peralkaline silicic derivatives can be produced by low pressure fractionation of a metaluminous trachyte. The extensive fractionation from a common transitional basaltic magma parent that the production of pantellerite liquids requires is in line with the low temperature, CO_2-poor, and water-rich character documented for those rhyolites at Pantelleria and elsewhere. The fact that pantelleritic melt inclusions generally lack detectable CO_2 by FTIR (e.g., Gioncada and Landi, 2010; Lanzo et al., 2013), does suggest that most of the CO_2 has been lost by the time pantelleritic magmas are produced in the plumbing system.

3. Experimental methods

3.1 Starting materials

We selected two pantellerite samples with similar compositions (Table 1) but slightly different crystal content (about 10% volume), one representing the basal pumice fall of the Green Tuff eruption (GTP; P.I = 1.68) and one representing a younger pumice deposit ('Fastuca' eruption, FTP; P.I.=1.56), which was also used in the experiments of Di Carlo et al. (2010).

3.1.1 The Green Tuff pantelleritic pumice (GTP)

The Green Tuff basal fallout consists of a 70-80 cm thick layer of poorly sorted pumice with scarce lithics. The pumice has a crystal content of $\leq$ 10 vol% (vesicle free) and its mineral assemblage is dominated (in order of decreasing abundance) by alkali feldspar, with minor aenigmatite and clinopyroxene, with fayalite, and quartz found occasionally embedded in a glassy groundmass. Ilmenite can be found as a uncommon inclusion in aenigmatite phenocrysts, a texture reminiscent of the antipathetic relationship proposed between FeTi-oxides and aenigmatite (Carmichael, 1962). Euhedral to subhedral alkali feldspars are homogeneous in composition ($An_{<0.1}Ab_{65-64}Or_{35-36}$) with a maximum length of 1 mm. Clinopyroxene microphenocrysts (length <

0.5mm) classify as sodian augite ($Wo_{40}En_{10}Fs_{50}$, with Na ≈ 0.16 apfu) while aenigmatite microphenocrysts have nearly homogenous compositions with XTi [$Ti/(Ti+Fe_{tot})$] = 0.15-0.17.

3.1.2 Fastuca pantelleritic pumice (FTP)

The Fastuca unit is comprised of dense and variably welded near-vent pumice fall deposits, sometimes agglutinated to form lava-like layers (Rotolo et al., 2007; Di Carlo et al., 2010). The pumice has a crystal content close to 20 vol% (vesicle free) and has a mineral assemblage similar to that of GTP, dominated by alkali feldspar, aenigmatite and clinopyroxene, with fayalite, amphibole and quartz occurring in minor amounts. The groundmass is characterized by a few alkali feldspar microphenocrysts and alkali feldspar + aegirine microlites (<100 microns) embedded in a glassy matrix. Alkali feldspars (up to 3 mm length) have composition $An_{<0.1}Ab_{65-64}Or_{35-36}$. Sodian (Na ≈ 0.14 apfu) augite microphenocrysts (length ≤ 0.5 mm) have a composition of $Wo_{42}En_{04}$-Fs_{54} and microphenocrysts of aegirine are also present. Aenigmatite phenocrysts (up to 2 mm in length) and microphenocrysts also have nearly homogenous compositions with XTi = 0.15-0.17. Olivine has a composition of Fa_{91-96}, and amphibole classifies as ferrorichterite-arfvedsonite group following Leake et al. (1997).

3.2 Experimental methods and charges preparation

We performed ten crystallization experiments, the experimental conditions being selected on the basis of previous works carried out on peralkaline rocks of Pantelleria (White et al., 2005, 2009; Di Carlo et al., 2010; Romano et al., 2018). All experiments were performed at 1 kbar, between 680°C and 900°C, and redox conditions between ΔNNO-0.5 and -2.5.

Due to the low crystal content, GTP was finely crushed to a grain size 10-30 μm and the powder obtained was used directly as starting material, using the same procedure of Scaillet and Macdonald (2001; 2003; 2006) for Kenyan rhyolites. For FTP the starting material was prepared using a standard procedure for phase equilibrium studies (e.g., Di Carlo et al., 2006, 2010; Andujar

et al., 2015, Romano et al., 2018), which consists of fusing twice the rock powder in air at 1200°C for 3 hours, then grinding the glass obtained to a 10-40 μm powder mesh size. This technique produces a crystal-free homogeneous glass with a composition similar to the starting bulk rock material (Table 1), favouring the attainment of bulk equilibrium.

Experimental charges were prepared by loading sequentially distilled water, CO_2 (added as silver oxalate) and 30 mg of starting material into gold capsules (1.5 cm long, inner and outer diameters of 2.5 mm and 2.9 mm, respectively). The amount of fluid (demineralized water and CO_2) was maintained at 10 wt% of the starting material (3 ± 0.5 mg) while the mole fraction of water in the fluid [$XH_2O_{in} = H_2O/(H_2O+CO_2)$] was varied between 0.1 and 1; each run consisted of 4-5 capsules (charges) with different XH_2O_{in}. Once loaded, the capsules were weighted, welded and left for 10-20 minutes in an oven at 100°C, in order to homogenize the fluid within the capsules, and reweighed to check for leaks. After the experiment, capsules were reweighted and those with pre-post weight difference higher than 0.4 mg were excluded. About half of the experimental product recovered upon capsule opening was mounted in epoxy, polished and carbon-coated for subsequent SEM and electron microprobe analyses.

3.3 Experimental apparatus

Experiments were performed in internally heated pressure vessels at the Institut des Sciences de la Terre d'Orléans, France (CNRS/UO/BRGM-ISTO), working vertically and equipped with a Kanthal furnace. The pressurizing medium, a mixture of argon (Ar) and hydrogen (H_2), was loaded sequentially at room temperature using an Ar/H_2 ratio that allowed to reach the desired redox conditions into the vessel (Scaillet et al., 1992, 1995). Different Ar/H_2 ratios were used during the experiments so as to reach redox conditions either around the FMQ buffer (similarly to those explored by Di Carlo et al., 2010) or below it. During the experiments the pressure was continuously recorded by a transducer calibrated against the Heise-Bourdon tube gauge (± 20 bar) while the temperature was continuously controlled through two S-type thermocouples (± 5°C)

bracketing the sample holder. Run duration varied between 146 and 552 hours and each experiment was terminated by switching off the power supply while keeping constant pressure (isobaric quench), except for experiments above 800°C for which a drop-quench device was used (Roux and Lefevre, 1992).

3.4 fH_2, fO_2 and H_2O_{melt} in the experimental charges

The experimental redox conditions prevailing during the experiment were determined *a posteriori* through solid sensors loaded along with the other capsules. This method allows the determination of fO_2 to $\pm$ 0.01 log fO_2 (Taylor et al., 1992; Pownceby and O'Neill, 1994). This in turns allows the fH_2 inside the vessel to be determined through the dissociation reaction of water:

$$K_w = f°H_2O / (fH_2 \times fO_2^{1/2})$$

where K_w is the water dissociation constant from Robie and Hemingway (1995), $f°H_2O$ the fugacity of pure water at the P and T of interest (Burnham et al., 1969) and fO_2 is given by the sensor. Since redox conditions lower than FMQ cannot recorded by Co-Pd solid sensors (Taylor et al., 1992), for below-FMQ runs we used the empirical relation of Di Carlo et al. (2010) to calculate fH_2 during the experiments. This relation, established from numerous experiments performed using H_2 membranes at ISTO (Scaillet et al., 1992), states that the final H_2 pressure reached at P-T is 3 ± 1 times higher than the H_2 pressure loaded to the vessel at room temperature. It is worth noting that this empirical relationships is verified by experiments performed with solid sensors (Table 2). The fO_2 specific to each capsule was then computed using either $f°H_2O$ for H_2O-saturated charges or $fH_2O = f°H_2O \times XH_2O_{in}$ (moles) for those with CO_2. The average error of computed fO_2 is $\pm$ 0.2 log units. Redox conditions range from ΔNNO-0.5 to ΔNNO-2.5 for the GTP and from ΔNNO-1.3 to ΔNNO-2.5 for the FTP.

The determination of the water content in glass (H_2O_{melt}) was difficult in most crystal-bearing runs (using either the '*by difference*' method or FT-IR spectroscopy). Thus, H_2O_{melt} in CO_2-

bearing charges was computed as follows: we first annealed 4 water-saturated glasses (fH$_2$O = fH$_2$O°) at various pressures (up to 2 kbar) with FTP. Resulting glasses had dissolved water contents up to 5.2 wt%, as determined by Karl Fisher Titration. From these, we derived an empirical relationship between f°H$_2$O (following Burnham et al., 1969) and H$_2$O$_{melt}$ in the form f°H$_2$O = a(H$_2$O$_{melt}$ wt%)^b, with a = 67.72 and b = 1.84 determined by regression. This equation can be rewritten as H$_2$O$_{melt}$ (wt%)= (fH$_2$O°/67.72)$^{1/1.84}$. In CO$_2$-bearing charges, f°H$_2$O was replaced by fH$_2$O as before [fH$_2$O = f°H$_2$O x XH$_2$O$_{in}$ (moles)]. This procedure requires an assumption of ideal behaviour in the H$_2$O-CO$_2$ fluid phase and the H$_2$O$_{melt}$ values obtained must be considered as maxima (Di Carlo et al., 2010; Andujar et al., 2015, Romano et al., 2018). In some crystal-free charges (i.e. GTR1-GTR4 and GTR22) the water content was also measured using the '*by difference*' method (Devine et al., 1995) and the results obtained (Table 2) are consistent with calculations. The standards used for the "by-difference" method were the four pantelleritic hydrous glasses used above. The accuracy of by-difference method for H$_2$O$_{melt}$ is estimated to be ± 0.5 wt% (Devine et al 1995).

3.5 Analytical techniques

Experimental products were first characterised with the scanning electron microscope for preliminary phase identification. Quantitative analyses of mineral phases and glasses were then obtained by microprobe (Cameca SX-Five housed at ISTO-BRGM joint facilities in Orleans). The analytical conditions used were: acceleration voltage of 15 kV, sample current 6 nA and a 10 s peak counting time for each element. A focused beam was used for analysing mineral phases whereas the experimental glasses were analysed employing a defocused beam 10 μm or 5 μm, the latter only when the high crystal content prevented the use of a 10 μm beam size. Na and K were analysed first and a ρφ(z) correction was applied. There was negligible Na loss from the glasses analysed using a defocused beam.

4. Experimental results

4.1 General observations

A summary of the results of our experiments is presented in Table 2. Crystallization experiments performed in our study produce results with similar textural features observed in other experiments done with similar compositions (e.g., Scaillet and Macdonald, 2006; Di Carlo et al., 2010). Achievement of near-equilibrium conditions is suggested by (i) the homogeneous distribution of phases within the charges, (ii) the euhedral shape of crystals, (iii) the regular variations of crystal abundances and compositions as a function of T, H_2O_{melt} and fO_2, and (iv) homogeneous glass compositions. Crystallization experiments reproduced all mineral phases observed in natural pantellerite: clinopyroxene (Cpx), olivine (Ol), alkali feldspar (Afs), ilmenite (Ilm), aenigmatite (Aenig), quartz (Qz) and amphibole (Amph), in addition to glass and vesicles, the latter indicating fluid-saturation conditions during the experiments. The compositions of minerals and glasses were used to determine phase proportions (Table 2) via mass-balance (Albarède, 1995), yielding square residuals (R^2) generally $\leq$ 1. This suggests that (i) no major phases were overlooked and (ii) Na_2O contents of experimental glasses have been evaluated correctly.

4.2 Phase proportions

Phase proportions of both compositions obtained from mass-balance calculations are listed in Table 2; mass-balance calculation is missing for three charges (GTR3-4 GTR3-5 and GTR23-4) due to difficulties in analysing the residual glass. The amount of melt varies from 100 wt% to 36 wt% and is directly correlated with temperature and melt water content decrease (Figure 2a). Supra-liquidus conditions were attained at 900°C for the GTP and 800°C for the FTP while the most crystallised charges are those at T $\leq$ 750°C (Figure 2a). At decreasing temperature and H_2O_{melt}, alkali feldspar becomes the most abundant mineral phase reaching a mass proportion of 43 wt% in

the most crystallised charges (Figure 2b). The sum of iron-bearing mineral phases (clinopyroxene, olivine, aenigmatite, oxides and amphibole) never exceeds 11 wt% (Figure 2c) while quartz proportion ranges between 3 wt% and 9 wt%. It is worth noting that in FTP, amphibole crystallises at < 700°C but its proportion does not approach the 21 wt% obtained by Di Carlo et al., (2010) in their lowest temperature experiments (680°C). In contrast, the proportions of alkali feldspar and clinopyroxene are comparable to those obtained by Di Carlo et al., (2010) and Scaillet and Macdonald (2003, 2006), and similar to those reported from the natural samples.

4.3 Phase relationships

The experimental phase relationships of both starting compositions were established at 1 kbar pressure (P), with temperature (T) between 900 and 750°C for the GTP and between 800 and 680°C for the FTP.

4.3.1 Green Tuff pantellerite (GTP)

At 1 kbar and 900°C GTP charges are at supra-liquidus conditions regardless for melt water contents explored in this study. At 850°C clinopyroxene is the liquidus phase for H_2O_{melt} < 2.5 wt% (Figure 3a), followed by alkali feldspar at H_2O_{melt} ~1 wt%. At T ≤ 800°C clinopyroxene is the liquidus phase at water saturated conditions while alkali feldspar expands its stability field at 750°C becoming stable when H_2O_{melt} is ~ 4 wt%. At T = 800°C and H_2O_{melt} ≤ 2.5 wt%, quartz joins the phase assemblage, whereas aenigmatite becomes stable at 750°C and H_2O_{melt} ≤ 3 wt%. Amphibole is stable in all charges at T < 850°C regardless of the melt water content (Figure 3a).

4.3.2 Fastuca pantellerite (FTP)

At 800°C all charges are at supra-liquidus conditions for H_2O_{melt} >2 wt%. At 750°C, clinopyroxene and fayalite (Figure 3b) are the liquidus phases at H_2O_{melt} saturation conditions (~4.5 wt% H_2O_{melt}), joined by alkali feldspar at 4 wt% H_2O_{melt} and aenigmatite at 3 wt% H_2O_{melt} and quartz at 2.5 wt % H_2O_{melt}. At 680°C feldspar is stable under water saturated conditions, along with

amphibole, aenigmatite and clinopyroxene while quartz crystallises between 3 and 4 wt% H_2O_{melt}. Fayalite is not stable at 680°C. Magnetite has been observed only at 750°C and H_2O_{melt} close to the saturation. Ilmenite occurs at 750°C and water-rich conditions, being replaced by aenigmatite at low H_2O_{melt}. Similarly to fayalite, ilmenite is not present at 680°C.

4.4 Phase compositions

Experimental phase compositions are reported in Tables 3-10, whereas the compositional variations with P-T-fO$_2$ and H_2O_{melt} are shown in Figures 4 to 9 and discussed below.

4.4.1 Clinopyroxene

Experimental clinopyroxene have compositions in the range $En_{2.24-25.2} - Fs_{34.3-68.81} - Wo_{33.4-38.5}$ and XFe_{tot} [apfu Fe/(Fe+Mg)] between 0.54 and 0.97. Ca and Na contents vary from augite to aegirine-augite (Figure 4a, Table 3): pure aegirine end-member does not crystallise in our experiments even though it has been synthetized in similar compositions (Scaillet and Macdonald 2003; 2006; Di Carlo et al., 2010) at temperatures lower than 750°C. At a given temperature, changes in H_2O_{melt}, and thus fO$_2$, influence the XFe_{tot} in clinopyroxene (Figure 4b-c). In the GTP charges, at constant H_2O_{melt} a decrease in temperature of 50°C increases XFe from 0.60 to 0.80. In FTP, clinopyroxene crystallizes only at < 800°C and has XFe_{tot} in the range 0.89-0.97, the Fe-richer crystals being produced at 680°C. The Na$_2$O content in clinopyroxene ranges between 0.70 wt% and 2.3 wt% in GTP, and up to around 7 wt% in FTP, broadly increasing with increasing P.I. (Figure 4d). It worth noting that clinopyroxene compositions synthetized at 750°C reproduce the small compositional range displayed by natural clinopyroxenes. The average clinopyroxene-liquid exchange coefficient ($K_d^{Mg-Fe}{}_{cpx-liq}$) calculated using FeO = FeO$_{tot}$ is 0.18 ± 0.03, which overlaps with the values found by and Di Carlo et al., (2010) ($K_d^{Fe-Mg}{}_{cpx-liq} = 0.16 ± 0.14$).

4.4.2 Olivine

Experimental olivine, synthesized only in the experiments performed on FTP, is fayalitic ranging from Fa_{90} to Fa_{93} (Table 4, Figure 5). The compositional range of experimental olivine perfectly matches that of corresponding phenocrysts in pantelleritic rocks (White et al., 2005; Civetta et al., 1998), having MnO contents up to 6.4 wt% (for a tephroite component as high as 6 mol%). Iron content increases with decreasing H_2O_{melt} and fO_2, while the Mn content roughly shows the opposite behaviour. The average exchange coefficient Kd^{Fe-Mg}_{ol-liq}, calculated with FeO = FeO_{tot}, is 0.58 ± 0.2. Considering instead the Fe^{2+}/Fe^{3+} of the melt, estimated with the method of Kress and Carmichael (1991) at the experimental T-fO_2, the K_d^{Fe-Mg} is 0.72 ± 0.2. In both cases the large standard deviation is associated with low MgO concentration (Table 4) in the melt. The K_d calculated using olivine phenocrysts and the glassy groundmass is K_d^{Fe-Mg} = 0.40 ± 0.1 (this work and data from Neave et al., 2012), which is at the lower end of that determined experimentally. The difference between the canonical Kd Ol-Liquid value of 0.30 (e.g., Roeder and Emslie, 1970; Toplis, 2005) and our calculated figures possibly comes in part from the insufficient calibration of Kress and Carmichael method for calculating the Fe2+/Fe3+ ratios of peralkaline silicic liquids at low fO_2 (Gaillard et al., 2001).

4.4.3 Fe-Ti oxides

Due to the small size, Fe-Ti oxides were analysed only in FTP experiments, in particular in the run GT-R20-3 (Table 5), in other experiments the analyses were strongly contaminated by the glass. Ilmenite in charge GT-R20-3 has an average FeO_{tot} = 44.9 ± 1.6 wt% and TiO_2 = 48.1 ± 0.7 broadly similar to the ilmenite composition of natural pantellerites.

4.4.4 Aenigmatite

Experimental aenigmatite (Table 6) has a fairly constant composition, matching that of corresponding phenocrysts in the natural samples. TiO_2 contents range between 7.3 wt% and 9.1 wt% while Na_2O contents vary between 6.8 wt% and 7.1 wt%, the latter showing no correlation

with P.I. However, as observed by Mahood and Stimac (1990) for Pantelleria pantellerites, Ca and

Al contents in aenigmatite decrease as P.I. increases. XTi=[Ti/(Fe+Ti)] ranges between 0.14 and

0.17 showing a positive correlation with temperature (Figure 6) and a negative correlation with fO_2.

4.4.5 Amphibole

Following the classification of Leake et al. (1997), experimental amphibole (Table 7) is

richterite – ferri-winchite, with a few charges also classifying as arfvedsonite. The amphibole

crystallising at 800°C in the GTP is ferri-winchite whereas at 750°C it ranges between ferri-

winchite and ferrorichterite. At fixed temperature a decrease of H_2O_{melt} increases the XFe and Na_2O

content (Figure 7a-b) while CaO shows the opposite behaviour (Figure 7c). In contrast, no

correlation exists between Al and K and experimental variables (i.e., temperature and H_2O_{melt}). It is

worth noting that the composition of the amphibole found in the Cuddia Mida products by White et

al., (2009) closely matches the composition of the experimental amphibole at 750°C (Figure 7c). In

FTP charges, amphibole crystallises only at 680°C (cf. Di Carlo et al., 2010) and its composition

corresponds to ferrorichterite-arfvedsonite. Compared with the composition of amphibole

crystallising at higher temperature, it represents the most enriched end-member in terms of Fe and

Na, matching also the amphibole composition of Fastuca pumices (Rotolo et al., 2007; Di Carlo et

al., 2010). Amphiboles crystallizing from GTP display higher F contents than those in FTP, Cl

contents being barely detectable in both cases.

4.4.6 Alkali feldspar

Analyses of experimental alkali feldspars are listed in Table 8 and range between $Or_{28.7-41.7}$-

$Ab_{52.8-70.6}$-$An_{0.0-0.4}$. The orthoclase content of alkali feldspar shows a broad positive correlation with

H_2O_{melt} and a negative correlation with temperature, in contrast to Ab and An, which broadly show

the inverse trend (note that the large errors associated with An content are due to the very low CaO

concentration). The variation in Or content with temperature is appreciable only at $\leq 750°C$ whereas

at higher temperatures a nearly horizontal trend in the range $Or_{28.7-41.7}$-$Ab_{52.8-70.6}$-$An_{0.0-0.4}$ is obtained (Figure 8). Overall, the lack of a clear correlation reflects the difficulties to analyse alkali feldspar in charges with low H_2O_{melt}, i.e. the charges with the highest crystal content. The composition of natural alkali feldspar in pantellerite is well reproduced at 750°C and H_2O_{melt} in the range 2.5-4 wt%.

4.4.7 Experimental glasses

The compositions of experimental glasses recalculated water-free are listed in Table 9. Following the classification of Macdonald (1974) all glasses are pantelleritic in composition, with 1.5 < P.I. < 2.5. The SiO_2 content ranges between 71 wt% and 75 wt%, whereas TiO_2, MnO, and CaO have concentrations always lower than 1 wt%, MgO concentration being lower than 0.1 wt%. FeO and Al_2O_3 contents range between 4.9 wt% - 9.3 wt% and 6.4 wt% - 9.9 wt%, respectively while Na_2O and K_2O vary between 6.1 wt% - 7.8 wt%, and 2.7 wt% - 4.9 wt%, respectively. The variation in glass composition with crystallization is shown in Figure 9. Glass composition in above-liquidus charges is similar to the composition of starting materials, whereas, as crystallization proceeds, FeO and Al_2O_3 vary notably, being inversely correlated to each other, SiO_2 remaining roughly constant. In detail, in the GTP charges SiO_2 and FeO show first a slight decrease then both increase again when the crystal content is > 10 wt%, while Al_2O_3 content shows the opposite behaviour (Figure 9a-c). As a result, the P.I. first becomes slightly lower than that of the starting material and then increases up to 2.1, being positively correlated with crystal content. Di Carlo et al. (2010) explained this behaviour (initial decline of P.I.) as due to the crystallization of mafic phases only, such as clinopyroxene (i.e., charges at $T \geq 800$°C and high H_2O_{melt}). In FTP, the SiO_2 content remains quite constant even though at 680°C SiO_2 is slightly higher than that at 750°C (Figure 9a). The FeO content increases with crystal content, reaching higher values at 750°C (6.3 wt% - 9.2 wt%) than at 680°C (5.4 wt% - 8 wt%, Figure 9b). With regards the Al_2O_3 content, it shows the opposite behaviour; consequently, the melt peralkalinity increases, the P.I. reaching a

value as high as 2.5 in the most crystallised charge analysed (#GT-R23-3). These melt evolutions

are shown in Figure 9d, using a ternary diagram $FeO-Al_2O_3-(Na_2O+K_2O)$ (moles), which depicts

the liquid lines of descent for fayalite-bearing charges (750°C) and for those bearing

amphibole+aenigmatite (680°C). In both cases, the liquids trend away from the peraluminous-

peralkaline divide line as a result of extensive alkali feldspar fractionation (see also Scaillet and

Macdonald, 2003).

5. Discussion

5.1 Comparison with previous experimental works

Previous experimental studies on peralkaline rhyolite include those of Scaillet and

Macdonald (2001, 2003, 2006) on Kenyan comendites (Olkaria) and pantellerites (Eburru), and

those of Di Carlo et al. (2010) on Pantellerian pantellerites, which used one of the same starting

pantelleritic materials (FTP) used in this study. The main differences between the Kenyan

comendites and the pantellerites, as described by Di Carlo et al. (2010) and confirmed in this study

concern: (i) the crystallization sequence and (ii) the stability of the mineral phases. Kenyan

pantellerites and comendites are more SiO_2-rich than pantellerites of Pantelleria and first crystallise

quartz and alkali feldspar, whereas clinopyroxene is the liquidus phase in Pantellerian pantellerites,

in part because the starting material is richer in CaO. Macdonald et al. (2011) suggested a possible

role for Cl and F as well, based on the effect of F on the Quartz-Orthoclase-Albite system (e.g.,

Manning et al., 1981) which expands the stability field of quartz over that of albite. Thus, Kenyan

peralkaline rhyolites, characterized by a high F/Cl ratio, reach quartz-feldspar cotectic earlier than

other peralkaline rhyolite systems (e.g., Pantelleria, Mayor Island, Azores), where Cl exceeds F and

quartz appears rarely, only as microphenocryst. Clinopyroxene crystallises over the whole range of

peralkaline silicic magma compositions and shows a wide compositional range, from Na-

hedenbergite to aegerine-augite and aegerine, although the latter is never found as phenocrysts but

only as microlites in groundmass (Macdonald et al., 2011). Scaillet and Macdonald (2006) and Di

Carlo et al. (2010) both synthetized aegirine at temperatures lower than 700°C while in our experiments aegirine never formed. Scaillet and Macdonald (2001) described the replacement of amphibole by aegirine at high fO_2; we infer therefore, that redox conditions in our experiments at 680°C are probably too reducing to allow aegirine to crystallise at this temperature, aegirine likely being only stable below 680°C. The slightly lower redox conditions (as compared to Di Carlo et al., 2010) explored in our study allowed the reproduction of Ca-rich clinopyroxene with XFe values perfectly matching those of the Fastuca sample when temperature is 750°C and H_2O_{melt} in the range 3 wt% - 4.5 wt%. The compositional differences observed in clinopyroxenes of the Green Tuff and Fastuca pantellerites (Table 2, Figure 4) can thus be reproduced at the same temperature (750°C) but at slightly different redox conditions.

Although aenigmatite occurs as phenocrysts in Eburru pantellerites it was not found in the experiments of Scaillet and Macdonald (2006), however, in the experiments of Di Carlo et al. (2010) as in our experiments, aenigmatite is found to be stable at $\leq$ 750°C for H_2O_{melt} poor-conditions and at 680°C under water-saturation conditions. The difference between the experimental results and Eburru pantellerites remains still unclear since the melt peralkalinity index, temperature and redox conditions are comparable. One possibility is a difference in pressure, which may have been slightly too low for the Kenyan experiments (1.5 kb): the results of Di Carlo et al. (2010) shows indeed that aenigmatite stability field shrinks at low pressure, this mineral being almost absent at 0.5 kb. In detail, note also that our FTP starting material is slightly Na_2O-richer than the one used by Di Carlo et al. (2010), by about 1 wt%, which could explain the larger stability field of aegnimatite in our FTP experiments, as anticipated from theoretical considerations on equilibria governing aenigmatite stability in peralkaline rhyolites (see section 5.3.2 below).

Fayalite (Fa_{92-94}) was synthesized at temperatures between 693-729 °C and fO_2 between ΔNNO-1.8 and ΔNNO-3.2 in Kenyan comendite (Scaillet and Macdonald 2003) while in Pantelleria trachyte the stability range of Fe-rich olivine (Fa_{60} to Fa_{88}), was established in the temperature

interval 750°C - 950°C over a similar redox range (ΔNNO-1.6 to ΔNNO-2.7; Romano et al., 2018).

We note that this is the first time that the stability field of fayalite (Fa_{90-93}) has been experimentally

established for pantellerite magmas. Our experimental results on Fastuca Pantellerite suggest that

the crystallization of fayalite in peralkaline silicic magmas depends on a subtle combination of

temperature, fO_2 and melt peralkalinity: for FTP it is restricted to temperatures between 690°C-

750°C, provided that the peralkalinity of melt and fO_2 allows it. The lack of olivine in GTP

experiments is interpreted to reflect that fO_2 was more oxidizing as compared to the natural system.

Such a restricted or highly sensitive stability field for fayalitic olivine is in contrast to what is

observed in peralkaline phonolites, where it occurs over a wider range of temperatures (Giehl et al.,

2013), and metaluminous rhyolites (Almeev et al., 2012). From a broader perspective, the

intermediate position of fayalitic olivine in the crystallisation interval (i.e. at intermediate

temperatures) of FTP is coherent with the observation that iron-rich olivine is present midway in

assemblages crystallising along the general liquid line of descent between trachytes and peralkaline

rhyolites, as further detailed below in section 5.2.

Factors controlling the stability of amphibole in pantellerites appears more difficult to

determine because of the scarce occurrence and wide compositional range of this mineral. Nicholls

and Carmichael (1969) and Conrad (1984) evidenced the role played by high fF_2 in favouring

amphibole stability (F-ferro ichterites to arfvedsonite). The experimental works of Scaillet and

Macdonald (2001, 2006) and Di Carlo et al. (2010) reported sodian amphibole being stable at T≤

750°C and pointed out that high fF_2 enhances its stability even in H_2O-poor magmas. Amphibole in

GTP displays F contents around 2 wt%, while in FTP amphibole has F contents lower than 1 wt%

(Table 7), which supports such an effect. Another factor that could explain the higher thermal

stability of amphibole in GTP is its higher Na_2O content relative to that of FTP and Kenyan

pantellerites. As for aenigmatite, our slightly richer Na FTP composition displays a slightly larger

(toward H_2O-rich conditions) stability field of amphibole as compared to that defined by Di Carlo et

al. (2010), which does suggest that Na stabilises amphibole in peralkaline rhyolites. Elevated Na_2O contents have been shown also to promote amphibole stability in calc-alkaline magmas (Sisson and Grove, 1993). Similarly, recent phase equilibria in metaluminous granites have shown that elevated Na_2O/K_2O ratios favour calcic amphibole crystallisation (Huang et al., 2019) and we suggest that this effect may apply to Na amphibole in peralkaline rhyolites as well.

Overall, our experimental results on GTP and those on FTP of Di Carlo et al. (2010) were both performed under a similar range of temperature and redox conditions, but the results of each have significant differences (as already noted for amphibole), in particular for minor phases. For instance, in the GTP experiments, clinopyroxene crystallises at 800°C and H_2O_{melt} close to the saturation conditions (H_2O_{melt} 4.5 wt%) while in the experiments of Di Carlo et al. (2010), clinopyroxene appears stable at the same temperature and pressure conditions but at H_2O_{melt} <4 wt %. This comparison shows that although the bulk-rock composition appears similar, the phase stabilities of minor phases are not, being extremely composition – specific and sensitive to even small variation in major elements or intensive parameters as already shown for phonolites or dacites (Scaillet et al., 2008, 2016; Andujar and Scaillet, 2012; Cadoux et al., 2014).

5.2 Comparison with results from natural samples and experiments

In addition to experimental studies, there have been several studies of the thermodynamic constraints on phase assemblages in natural pantellerites. These previous studies on natural pantellerites have established the efficacy of the Ca-QUIlF (quartz-ulvöspinel-ilmenite-fayalite; Frost et al., 1988; Andersen et al., 1993) system to provide information on temperature, oxygen fugacity, and silica activity from equilibrium assemblages of clinopyroxene-olivine-oxide that compares favourably with both other thermobarometric methods (e.g., two oxides, clinopyroxene-glass; White et al., 2005; Liszewska et al., 2018) and experimental results (Scaillet and Macdonald, 2003, 2006; Di Carlo et al., 2010; Romano et al., 2018). Geothermobarometric results presented by previous studies have been recalculated for P = 1000 bars for consistency and comparison with

experimental work, and to add silica activity where none was reported previously. These results are summarized in Table 10 and the full results of the QUILF95 program are presented in Supplementary Table 1. Amongst both recent and earlier studies (e.g., Carmichael, 1962, 1966; Nicholls and Carmichael, 1969) particular attention has been paid to the stability of aenigmatite and amphibole, their apparent antipathetic relationship with fayalite, and the nature of the so-called "no oxide field" in strongly peralkaline rocks. In general, these recent studies have established a "reaction series" for the liquid line of descent from trachyte (P.I. ≈ 1.0) to pantellerite (P.I. ≈ 2.0): (i) augite (apfu [atoms per formula unit] Ca+Na < 0.90) + olivine + ilmenite + magnetite; (ii) sodian augite (apfu Ca+Na < 0.90, apfu Na > 0.10) + fayalitic olivine + one oxide; (iii) sodian hedenbergite (apfu Ca+Na > 0.90, apfu Na > 0.10, XFe_{tot} [Fe_{tot}/(Fe_{tot}+Mg)] > 0.50) + fayalite + one oxide + aenigmatite; (iv) sodian hedenbergite + one oxide (typically ilmenite) + aenigmatite + quartz ± amphibole; and (v) aegirine-augite (apfu Na > 0.20, XFe_{tot} > 0.50) + aenigmatite + quartz ± amphibole, with the final assemblage representing crystallization in the "no-oxide" field. Alkali feldspar is common to each assemblage described above. Reactions describing these relationships are presented in Table 11. Additionally, with decreasing temperature the natural assemblages also record gradually increasing silica activity and more oxidizing conditions relative to the NNO buffer (from ΔNNO-2 to ΔNNO-0.9) which may be related to increasing water concentrations in the more evolved pantellerites at Pantelleria (cf., Liszewska et al., 2018; Romano et al., 2019). In contrast, mineral assemblages in the Kenyan pantellerites record silica activities and oxygen fugacities that remain nearly constant ($aSiO_2$[Qz] ≈ 0.7 and ΔNNO-2 at Menengai and $aSiO_2$[Qz] ≈ 0.9-1.0 and ΔNNO-2.0 to -1.5 at Eburru; Ren et al., 2006; Macdonald et al., 2011). The experimental results on FTP at 1 kbar and fO_2 < FMQ (Fig. 3b) result in a very similar crystallization sequence. Starting from a liquidus temperature of 800°C, a decrease in temperature to ~750°C results in the crystallisation of clinopyroxene, alkali feldspar, olivine, magnetite, and ilmenite. As temperatures continue to decrease, magnetite ceases to crystallise, which is followed by the appearance of aenigmatite, and then a loss of olivine and ilmenite. Quartz crystallizes early under lower-water

(<3.5 wt%) conditions and not at all at higher-water conditions, whereas amphibole crystallizes at ~700°C over a wide range of water concentrations. For a narrow range of temperature, redox conditions (ΔNNO-1.92), H_2O_{melt} and $aSiO_2$ the experiments reproduced mineral phases and assemblages very similar to the mineral assemblages (i), (ii) (iii) described above. Fayalite and ilmenite at more reducing conditions disappear (ΔNNO < - 1.92), realistically, as the result of the antipathetic relations with aenigmatite and projecting the peralkaline magma toward the crystallization in the "no-oxide field". The transition in the mineral assemblage described is driven by a progressive increase of the melt peralkalinity and $aSiO_2$. This latter is confirmed by the quartz as stable phase. Mineral assemblages (iv) and (v) present quartz ± amphibole, following the phase diagram in Fig. 3b this one can be realized when peralkaline magma at crystallization temperature lower than 680°C. Crystallization at T≤680° would also explain the presence of aegerine, never synthetized in our experiments but stable in the experiment of Scaillet and Macdonald (2006) and Di Carlo et al. (2010) at temperature lower than 680°C. Scaillet and Macdonald (2001) evidenced a replacement of Na-amphibole by aegirine at increasing fO_2 evidenced while Marks et al. (2003) proposed an antipathetic reaction between aegirine and arfvedsonite, these consideration may explain the more oxidising conditions determined for mineral assemblage (v). In the following paragraphs will be reported the theoretical calculation obtained on pantellerite magmas.

5.2.1. Clinopyroxene and olivine

Along with alkali feldspar, clinopyroxene is a nearly ubiquitous phase in phyric pantelleritic rocks, changing in composition with increasing peralkalinity from augite to sodian augite/hedenbergite to aegirine-augite in samples from Pantelleria (White et al., 2005, 2009). In contrast, the clinopyroxenes reported from Eburru are nearly all sodian (apfu Na ≥ 0.12) hedenbergite to aegirine-augite and those reported from Menengai are low Na (<0.08 apfu) augite and hedenbergite. Di Carlo et al. (2010) described a strong negative correlation between XFe_{tot} in

clinopyroxene, temperature, and oxygen fugacity from their experimental results; a similar regression can be derived from the natural data from Pantelleria, Menengai and Eburru:

$$XFe_{tot} = 1.972 - 0.00135 \cdot T(°C) - 0.0403 \cdot \log fO_2 \ (n = 27, R^2 = 0.77, SE = 0.08) \ (Eqtn\ 1)$$

The composition of olivine ranges from ~72 mol% Fa in trachytes (P.I. ≈ 0.95) to ~99 mol% in pantellerites, although its presence is not as nearly common as clinopyroxene. At Pantelleria, it is present in all samples with P.I. < 1.62 and T ≥ 736°C with a single reported occurrence in a sample from Cuddia Mida (95 mol% Fa) with P.I. = 1.82 and T = 718°C. Olivine is present in all but one of the samples reported from Eburru and Menengai. At Eburru it is nearly pure fayalite (98.8-99.6 mol% Fa) and occurs with ilmenite and aenigmatite at low (684-721°C) temperatures; at Menengai it ranges from 77.7-83.2 (with a single outlier at 96.8) mol% Fa where it forms an aenigmatite-free assemblage with spinel at higher (793-867°C) temperatures. Both the experiments and the natural samples are in good agreement on the limited temperature range for the stability of fayalite in pantellerites.

The composition of olivine has small negative associations with both temperature and oxygen fugacity ($R^2 \approx 0.65$), but a strong positive correlation with the iron content of equilibrium clinopyroxene (XFe_{tot}):

$$Fa \ (mol\%) = 47.21 + 54.68 \cdot XFe_{tot} \ (n = 22, R^2 = 0.96, SE = 1.9), \ (Eqtn\ 2)$$

which we propose may be used as a test for equilibrium between clinopyroxene and olivine pairs in pantelleritic rocks.

Furthermore, Romano et al. (2018) proposed an equation to parameterize the influence of T, H_2O_{melt} and fO_2 on olivine composition in trachytic magma compositions. Here, considering the continuous compositional trend with Fe-rich olivine in trachyte, we present a modified equation that takes into account the new experimental data:

$$\text{Fa (mol\%)} = -0.1720*T(°C)-6.6176*\Delta NNO-0.3715*H_2O_m+212.1635 \qquad (R=0.93) \quad \text{(Eqtn 3)}$$

Equation (3) back-calculates the Fa content of experimental olivine to within 1.7 mol % and is valid for trachytic to pantelleritic magma compositions. For instance, if we take into account the average water content in fayalite melt inclusions (Gioncada and Landi, 2010) and redox conditions reported by White et al. (2005) for composition Fa_{85-97} the equation back-calculates temperatures in the range 715-783 °C.

5.2.2. Iron-Titanium Oxides

The paucity of oxide pairs and the preponderance of ilmenite over magnetite in mineral assemblages in pantelleritic rocks has been long recognized (Carmichael, 1962). Although magnetite is less common in samples from Pantellerie and Eburru, it is the dominant oxide at Menengai. In general, magnetite occurs as the sole oxide phase in pantellerites that equilibrated with olivine (>70 mol% Fa) and low-Na clinopyroxene (<0.08 apfu Na, XFe_{tot} = 0.45-0.84) over a wide range of silica activities relative to quartz saturation ($a_{SiO2}[Qtz]$ = 0.6 – 0.9) at relatively high temperatures (904-793°C), with ulvöspinel (Usp) compositions ranging from 64 to 79 mol%. By contrast, with the exception of a single outlier (sample 150551) ilmenite is the sole oxide phase in equilibrium with more fayalitic olivine (>85 mol% Fa) and more sodian clinopyroxene (0.07-0.22 apfu Na, XFe_{tot} = 0.69-0.93) over a much narrower range of $a_{SiO2}[Qtz]$ (>0.9) and wider range of temperature (899-684°C), with only minor variation in composition (93-97 mol% Ilm). Both oxides occur over a similar range of oxidation state, although magnetite appears limited to oxygen fugacities below ΔNNO-1.3. The experiments of Di Carlo et al., (2010) synthetized magnetite in an oxygen fugacity range of ΔNNO-0.53 and ΔNNO-1.06. In this study ilmenite (ilm mol% = 95.4) is stable at 750°C for redox conditions ΔNNO-1.52 and ΔNNO-1.92. The compositions of each have negative associations with ΔNNO (Figure 10) and can be approximated by:

$$\text{Ilm (mol\%)} = 91.35 - 2.703 \cdot \Delta NNO \; (n = 20, R^2 = 0.85, SE = 0.57), \qquad \text{(Eqn 4) and}$$

$$\text{Usp (mol\%)} = 48.06 - 13.73 \cdot \Delta NNO \ (n = 11, \ R^2 = 0.75, \ SE = 2.5). \qquad \text{(Eqn 5)}$$

Due to their occurrence over a similar range of temperature and oxygen fugacity, we propose that silica activity exerts the greatest control on whether ilmenite or magnetite will crystallise, as described by QUIlF (Frost et al., 1988):

$$2Fe_2TiO_4 + SiO_2 = 2FeTiO_3 + Fe_2SiO_4$$

$$2Usp + Q = 2Ilm + Fa.$$
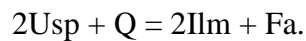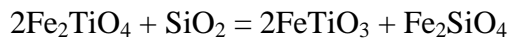
This reaction and the results from Table 11 are plotted in Figure 11. Figure 11a shows the position of the QUIlF curve calculated using the activites of ilmenite, ulvospinel, and fayalite from the sole two-oxide pantellerite (sample 98520, White et al., 2005, 2009). As noted by Markl et al. (2010), this reaction shows that magnetite will be favoured at lower silica activities and higher temperatures. For lower activities of fayalite in olivine, the curve will be displaced to even higher temperatures, whereas more oxidizing conditions (and corresponding lower Usp and Ilm activities) will displace this curve to lower temperatures, expanding the stability of spinel in pantellerites. Therefore, it may be under these lower-temperature and more oxidizing (approaching NNO) conditions that the rare aenigmatite+magnetite assemblage variety of assemblage (iv) occurs.

In contrast with the natural samples, experimental results tend to produce magnetite instead of both ilmenite and fayalite. This is because experimentally applied fO_2 is in general higher than the one prevailing in nature. Additionally, experimental results tend to produce clinopyroxene with much higher aegirine contents than found in the natural samples.

5.2.3. Aenigmatite

Aenigmatite occurs in assemblages with ilmenite and olivine (>92 mol% Fa) over a wide range of temperature (<800°C) and oxygen fugacities (ΔNNO-2.1 to ΔNNO-0.9), but only at high silica activities where it frequently occurs in assemblages with quartz. The control of silica activity

on aenigmatite crystallization has also been noted by Macdonald et al. (2011, 2019), who described

the antipathetic relationship between fayalite and aenigmatite as:

$$\tfrac{1}{2}FeTiO_3 + Fe_2SiO_4 + \tfrac{1}{2}Na_2Si_2O_5 + SiO_2 = \tfrac{1}{2}Na_2TiFe_5Si_6O_{20}$$

$$\tfrac{1}{2}Ilm + Fa + \tfrac{1}{2}Nds + Q = \tfrac{1}{2}Aen.$$
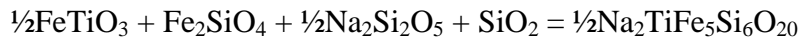
This reaction is plotted in Figure 11b. The position of the curve as plotted is based on the activities

of ilmenite, and fayalite from the highest-temperature sample with the fayalite-ilmenite-aenigmatite

assemblage (the tuhualite-bearing 160541; Bagiński et al., 2018). All curves are calculated with

aNds (melt) = 1.0, which may be assumed for strongly peralkaline rocks (Carmichael et al., 1974;

White et al., 2005). Lower activities of either ilmenite (suggesting oxygen fugacities closer to

NNO) or fayalite displaces this curve to lower temperatures. We present an alternate expression of

this reaction that includes an explicit role for oxygen fugacity (Figure 11c),

$$\tfrac{1}{3}FeTiO_3 + \tfrac{1}{3}Fe_2O_3 + \tfrac{1}{3}Fe_2SiO_4 + \tfrac{1}{3}Na_2Si_2O_5 + SiO_2 = \tfrac{1}{3}Na_2TiFe_5Si_6O_{20} + \tfrac{1}{6}O_2$$

$$\tfrac{1}{3}Ilm + \tfrac{1}{3}Hem + \tfrac{1}{3}Fa + \tfrac{1}{3}Nds + Q = \tfrac{1}{3}Aen + \tfrac{1}{6}O_2.$$
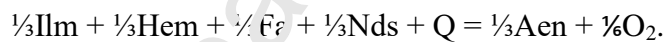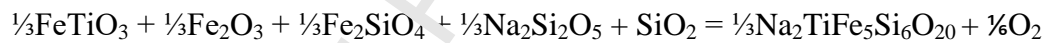
The equation for this calculation is presented in Table 11 and was derived from the data used by

Macdonald et al. (2011) reproducing also the result of the previous reaction well and demonstrates

dual roles of high silica activity and low oxygen fugacity on aenigmatite stability. The ilmenite-out

reaction (viz., "no-oxide field") was described by White et al. (2005) as a function of temperature

and oxygen fugacity and recast as a function of these plus silica activity by Macdonald et al. (2011):

$$\tfrac{1}{4} FeTiO_3 + \tfrac{1}{2} Fe_2O_3 + \tfrac{1}{4} Na_2Si_2O_5 + SiO_2 = \tfrac{1}{4} Na_2TiFe_5Si_6O_{20} + \tfrac{1}{4} O_2.$$

$$\tfrac{1}{4}Ilm + \tfrac{1}{2}Hem + \tfrac{1}{4}Nds + Q = \tfrac{1}{4}Aen + \tfrac{1}{4} O_2.$$
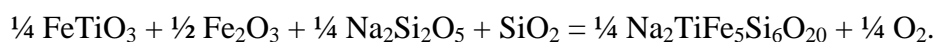
This reaction is plotted in Figure 11d with curves representing oxygen fugacities from ΔNNO-2 to ΔNNO-0.9 (with ilmenite compositions calculated with equation 4 above), representing the range of conditions from Table 10.

5.2.4. Amphibole

Amphibole is an uncommon phase at Pantelleria, having been reported only occasionally from pre-Green Tuff ignimbrites (Jordan et al., 2018) and from the younger lavas and tuffs related to Cuddia Mida and Fastuca on the northern slopes of Montagna Grande (Rotolo et al., 2007; White et al., 2009). In contrast, amphibole is a common phase in Eburu pantellerites, In both cases, it occurs in assemblages with aenigmatite, ilmenite, and clinopyroxene at temperatures <730°C and oxygen fugacities between ΔNNO-0.9 and ΔNNO-2.1. The experimental results of Charles (1977) suggest that the stability of amphiboles in the richterite-ferrorichterite solid solution series expands to higher temperatures as a function of higher Mg content and lower oxygen fugacity. For example, at oxygen fugacities defined by the FMQ buffer (ΔNNO-0.75), the end-member ferrorichterite ($XFe_{tot} = 1.0$) is stable at temperatures below 535°C, which increases with increasing Mg to 730°C ($XFe_{tot} = 0.8$), 910°C ($XFe_{tot} = 0.6$), and up to 1025°C ($XFe_{tot} = 0.0$). With decreasing oxygen fugacity, the stability of end-member ferrorichterite increases from 535°C (ΔNNO-0.75) to 760° (ΔNNO-4). Sample 98527 (Scirafi, Pantelleria, White et al., 2009) has amphibole with $XFe_{tot} \approx 0.8$, which is stable at 730°C at NNO-0.75; this is consistent with the calculated temperature (729°C) and oxygen fugacity (ΔNNO-0.88). The other reported natural amphiboles have $0.92 < XFe_{tot} < 0.98$, with calculated temperatures <720°C and oxygen fugacities between NNO-1.0 and NNO-2.1 (Figure 12).

5.3 Implications for the Pantelleria magmatic system

Further constraints on pre-eruptive redox conditions and temperatures of pantellerite magmas of Pantelleria can be gained from our results. As already pointed out by Di Carlo et al.

(2010), the P-T stability of aenigmatite represents the main phase equilibrium argument to constrain the pre-eruptive temperature of pantellerites at about $730\pm10°C$ and redox conditions between NNO-0.5 and NNO-2.0. Our findings, which show that olivine displays a thermally restricted stability field at $750\pm20°C$ (for H_2O_{melt} in the range 3-4.5 wt%), is in full agreement with such an estimate. Alkali feldspar, clinopyroxene and olivine compositions are also successfully reproduced at around 750°C. At lower temperature (i.e., 680°C) mineral phases are more evolved (i.e., Fe-rich Ol/Cpx or Or-rich Afs) than their natural counterparts. It may be noted that at 750°C and H_2O_{melt} ranging between 3 wt% and 4.5 wt% the crystal content of experimental products is similar to that observed in natural pantellerites while at 680°C it increases from 30 wt% to 63 wt%. We stress here that crystal contents of erupted material could be altered by transport processes associated to magma segregation and up rise. But if equilibrium experiments do reproduce them, then the implications are that equilibrium prevailed in the reservoir and that the dynamic associated to melt extraction and eruption maintained crystal proportions up to the surface.

Melt inclusion studies (Gioncada and Landi 2010; Neave et al., 2012; Lanzo et al., 2013) have reported a slightly lower average water content (H_2O_{melt} =2.6 ± 1.2 wt% for 80 MI analysed), yet H_2O_{melt} ranges between 1.3 wt% and 4.9 wt%. The low end of this range of H_2O_{melt} possibly reflects diffusional loss of water from the inclusion during magma uprise and eruption. In support of this is the fact that most of melt inclusions are hosted by alkali feldspar which has a quite homogeneous composition (Ab_{65}-Or_{35}), which in our experiments is produced at 750°C, 1 kbar and H_2O_{melt} = 3-4 wt% (Figure 8). In Figure 13 whole rocks and melt inclusions (MI) are compared with experimental glasses. Most of MIs fall close to, or on, the cotectic line defined by multiply saturated experimental charges at 750°C (i.e alkali feldspar, clinopyroxene, fayalite and aenigmatite-bearing charges), which gives further support to the above conclusion of a pre-eruptive magma temperature around 750°C.

Regarding amphibole and its rare occurrence in Pantelleria rhyolites, Di Carlo et al. (2010) suggested that it crystallises from a wetter and possibly deeper storage region. In this way, amphibole would coexist with alkali feldspar for crystal contents comparable with those observed in natural pantellerite. On the basis of our experimental results, an alternative explanation would be that amphibole and alkali feldspar coexist at T> 680°C in pantelleritic magmas with high fF_2. Regardless the strong correlations existing between the CaO/Na$_2$O contents of amphibole and H$_2$O$_{melt}$ (Figure 7a,b) indicate that melt water content during amphibole crystallisation was in the range 3-4 wt%, if the magma was at 750°C, in agreement with the inferences made above.

6. Conclusions

This study was aimed at exploring the role of composition and fO_2 on pantellerite phase relationships by comparing experiments and thermodynamic modelling, along with recent results gathered on peralkaline rhyolites worldwide. Phase relationships and phase compositions show evident differences in relation both to small differences in whole-rock composition and to the imposed experimental parameters, in particular redox conditions. Our main findings can be summarized as follows:

1. The experimental results and thermodynamic modelling confirm that peralkaline rhyolite evolves at temperature $\leq 750°C$ prior to eruption.

2. For first time, the experiments successfully reproduced all mineral phases observed in pantellerites. In particular, the stability of fayalite has been experimentally constrained, at 1.0 kbar, 750°C, H$_2$O$_{melt}$ and redox conditions in the range NNO-1.3 to NNO-1.9. Experiments also confirm that amphibole is stable in peralkaline rhyolites at temperature $\leq 800°C$, being promoted by high fF_2.

3. As anticipated, redox conditions have an influential role on the stability fields of some mineral phases and liquidus temperature of pantellerites. A "reaction series" along the liquid line of descent of felsic peralkaline oversaturated magmas has been established by combining experimental

and thermodynamical constraints, variations in $a\mathrm{SiO_2}$ and $f\mathrm{O_2}$ exerting a prime control, in addition to temperature, melt water content and melt peralkalinity.

4. The data presented here can be considered in order to implement thermodynamic modeling software for phase equilibria in magmatic systems (e.g. Rhyolite Melts, Gualda et al., 2012) also for alkaline and peralkaline evolved magmas. Previous work has demonstrated (White et al., 2009; Romano et al., 2019) that such a model does not faithfully reproduce the transition between evolved pantelleritic and parental trachyte magmas.

Acknowledgements

References

Albarède, F., 1995. Introduction to Geochemical Modelling. Cambridge: Cambridge University Press, 543p.

Almeev, R.R., Bolte, T., Nash, B.P., Holtz, F., Erdmann, M., Cathey, H.E., 2012. High-temperature, low-H2O Silicic Magmas of the Yellowstone Hotspot: an Experimental Study of Rhyolite from the Bruneau–Jarbidge Eruptive Center, Central Snake River Plain, USA. Journal of Petrology 53, 1837–1866. https://doi.org/10.1093/petrology/egs035

Andersen J., L.D., H., D.D., M., P., 1993. QUILF: a Pascal program to assess equilibria among Fe-Mg-Mn-Ti oxides, pyroxenes, olivine, and quartz. Computers & Geosciences 19, 1333–1350. https://doi.org/10.1016/0098-3004(93)90033-2

Andújar, J., Scaillet, B., 2012 Experimental Constraints on Parameters Controlling the Difference in the Eruptive Dynamics of Phonolitic Magmas: the Case of Tenerife (Canary Islands). Journal of Petrology 53, 1777–1806, https://doi.org/10.1093/petrology/egs033

Andújar, J., Scaillet, B., Pichavant, M., Druitt, T.H., 2015. Differentiation Conditions of a Basaltic Magma from Santorini, and its Bearing on the Production of Andesite in Arc Settings. Journal of Petrology 56, 765–794. https://doi.org/10.1093/petrology/egv016

Avanzinelli, R., 2004. Crystallisation and genesis of peralkaline magmas from Pantelleria Volcano, Italy: an integrated petrological and crystal-chemical study. Lithos 73, 41–69. https://doi.org/10.1016/j.lithos.2003.10.007

Bagiński, B., Macdonald, R., White, J., Jeżak, L., 2018. Tuhualite in a peralkaline rhyolitic ignimbrite from Pantelleria, Italy. European Journal of Mineralogy 30, 367–373.

https://doi.org/10.1127/ejm/2018/0030-2711

Bailey, D.K., Schairer, J.F., 1966. The System Na2O−Al2O3−Fe2O3−SiO2 at 1 Atmosphere, and the Petrogenesis of Alkaline Rocks. Journal of Petrology 7, 114–170.

Bohrson, W.A., Reid, M.R., 1997. Genesis of Silicic Peralkaline Volcanic Rocks in an Ocean Island Setting by Crustal Melting and Open-system Processes: Socorro Island, Mexico. Journal of Petrology 38, 1137–1166. https://doi.org/10.1093/petroj/38.9.1137

Burnham, C.W., Holloway, J.R., Davis, N.F., 1969. Thermodynamic Properties of Water to 1,000° C and 10,000 Bars, in: Burnham, C.W., Holloway, J.R., Davis, N.F. (Eds.), Thermodynamic Properties of Water to 1,000° C and 10,000 Bars. Geological Society of America.

Cadoux, A., Scaillet, B., Druitt, T.H., Deloule, E., 2014. Magma Storage Conditions of Large Plinian Eruptions of Santorini Volcano (Greece). Journal of Petrology 55, 1129–1171. https://doi.org/10.1093/petrology/egu021

Carmichael, I.S.E., 1962. Pantelleritic liquids and their phenocrysts. Mineralogical Magazine and Journal of the Mineralogical Society, Volume 33, 86–113. https://doi.org/10.1180/minmag.1962.033.257.03.

Carmichael, I. S. E., 1966. The iron-titanium oxides of salic volcanic rocks and their associated ferromagnesian silicates. Contributions to mineralogy and petrology, 14(1), 36-64.

Carmichael, I,S,E., Turnerm F.J., Verhoogen, J., 1974 Igneous petrology. McGraw Hill, New York, N.Y.

Carmichael, I.S.E., MacKenzie W. S., 1963. Feldspar-liquid equilibria in pantellerites; an experimental study. American Journal of Science, 261(4), 382-396.

Charles, R. W., 1977. The phase equilibria of the intermediate composition on the pseudobinary $Na_2CaMg_5Si_8O_{22}(OH)_2$ - $Na_2CaFe_5Si_8O_{22}(OH)_2$. American Mineralogist 277, 594-625.

Chase, M.W., Jr., Davies, C.A., Downey, J.R., Jr., Frurip, D.J., McDonald, R.A., Syverud, A.N., 1985. JANAF Thermochemical Tables, 3rd Edition. Journal of Physical Chemistry Reference Data 14, supp. no. 1

Civetta, L., Cornette, Y., Gillot, P.Y., Orsi, G., 1988. The eruptive history of Pantelleria (Sicily channel) in the last 50 ka. Bulletin of Volcanology. 50, 47–57. https://doi.org/10.1007/BF01047508.

Civetta, L., D'Antonio, M., Orsi, G., Tilton, G., R., 1998. The Geochemistry of Volcanic Rocks from Pantelleria Island, Sicily Channel: Petrogenesis and Characteristics of the Mantle Source Region. Journal of Petrology 39, 1453–1491. https://doi.org/10.1093/petroj/39.8.1453.

Conrad, W.K., 1984. The mineralogy and petrology of compositionally zoned ash flow tuffs, and related silicic volcanic rocks, from the McDermitt Caldera Complex, Nevada-Oregon. Journal of Geophysical Research. 89, 8639. https://doi.org/10.1029/JB089iB10p08639.

Dall'Agnoll, R., Scaillet, B., Pichavant, M., 1999. An Experimental Study of a Lower Proterozoic A-type Granite from theEastern Amazonian Craton, Brazil, Journal of Petrology 40, Pages 1673–1698, https://doi.org/10.1093/petroj/40.11.1673.

Devine, J.D., Gardner, J.E., Brack, H.P., Layne, G.D., Rutherford, M.J., 1995. Comparison of microanalytical methods for estimating H_2O contents of silicic volcanic glasses. American

Mineralogist. 80, 319–328. https://doi.org/10.2138/am-1995-3-413.

Di Carlo, I., Pichavent, M., Rotolo, S., Scaillet, B., 2006. Experimental crystallization of a high-K arc basalt: The Golden Pumice, Stromboli Volcano (Italy). Journal of Petrology, 47, 1317-1343. https://doi.org/10.1093/petrology/egl011.

Di Carlo, I., Rotolo, S.G., Scaillet, B., Buccheri, V., Pichavant, M., 2010. Phase Equilibrium Constraints on Pre-eruptive Conditions of Recent Felsic Explosive Volcanism at Pantelleria Island, Italy. Journal of Petrology 51, 2245–2276. https://doi.org/10.1093/petrology/egq055

Huang, F., Scaillet, B., Wang, R., Erdmann S., Chen Y., Faure, M., Liu, H., Xie, L., Wang, B., Zhu, J., 2019. Experimental Constraints on Intensive Crystallization Parameters and Fractionation in A - Type Granites: A Case Study on the Qitianling Pluton, South China J. of Geophys. Res:Solid Earth,124, 1-12. https://doi.org/10.1029/2019JB017490

Frost, B.R., Lindsley, D.H., Andersen, D.J., 1988. Fe-Ti oxide-silicate equilibria; assemblages with fayalitic olivine. American Mineralogist. 73, 727–740.

Gaillard, F., Scaillet, B., Pichavant, M., & Bény, J. M., 2001. The effect of water and fO_2 on the ferric–ferrous ratio of silicic melts. Chemical Geology, 174(1-3), 255-273.

Giehl, C., Marks, M., Nowak, M., 2013. Phase relations and liquid lines of descent of an iron-rich peralkaline phonolitic melt: An experimental study. Contributions to Mineralogy and Petrology. 165, 283–304. https://doi.org/10.1007/s00410-012-0809-6

Gioncada, A., Landi, P., 2010. The pre-eruptive volatile contents of recent basaltic and pantelleritic magmas at Pantelleria (Italy). Journal of Volcanology and Geothermal Research 189, 191–201. https://doi.org/10.1016/j.jvolgeores.2009.11.006

Gualda, G., Ghiorso, M., RV, L., Carley, T., 2012. Rhyolite-MELTS: a Modified Calibration of MELTS Optimized for Silica-rich, Fluid-bearing Magmatic Systems. Journal of Petrology 53, 875–890. https://doi.org/10.1093/petrology/egr080

Jeffery, A. J., Gertisser, R., Self, S., Pimentel, A., O'Driscoll, B., Pacheco, J. M., 2017. Petrogenesis of the Peralkaline Ignimbrites of Terceira, Azores. J. Petrol, 58, 2365–2402, https://doi.org/10.1093/petrology/egy012

Jordan, N.J., Rotolo, S.G., Williams, R., Speranza, F., McIntosh, W.C., Branney, M.J., Scaillet, S., 2018. Explosive eruptive history of Pantelleria, Italy: Repeated caldera collapse and ignimbrite emplacement at a peralkaline volcano. Journal of Volcanology and Geothermal Research 349, 47–73. https://doi.org/10.1016/j.jvolgeores.2017.09.013

Kress, V.C., Carmichael, I.S.E., 1991. The compressibility of silicate liquids containing Fe_2O_3 and the effect of composition, temperature, oxygen fugacity and pressure on their redox states. Contributions to Mineralogy and Petrology. 108, 82–92. https://doi.org/10.1007/BF00307328

Lanzo, G., Landi, P., Rotolo, S.G., 2013. Volatiles in pantellerite magmas: A case study of the Green Tuff Plinian eruption (Island of Pantelleria, Italy). Journal of Volcanology and Geothermal Research 262, 153–163. https://doi.org/10.1016/j.jvolgeores.2013.06.011

Leake, B.E., Woolley, A.R., Arps, C.E.S., Birch, W.D., Gilbert, M.C., Grice, J.D., Hawthorne, F.C., Kato, A., Kisch, H.J., Krivovichev, V.G., Linthout, K., Laird, J., Mandarino, J., Maresch, W. V, Nickel, E.H., Rock, N.M.S., Schumacher, J.C., Smith, D.C., Stephenson, N.C.N., Ungaretti, L., Whittaker, E.J.W., Youzhi, G., 1997. Nomenclature of Amphiboles; Report of the Subcommittee on Amphiboles of the International Mineralogical Association Commission on

New Minerals and Mineral Names. Mineral. Mag. 61, 295–310. https://doi.org/10.1180/minmag.1997.061.405.13

Lindsley, D.H. (1971): Synthesis and preliminary results on the stability of aenigmatite ($Na_2Fe_5TiSi_6O_{20}$). Carnegie Institution Year Books 69, 188-190.

Liszewska, K., White, J., Macdonald, R., Bagiński, B., 2018. Compositional and Thermodynamic Variability in a Stratified Magma Chamber: Evidence from the Green Tuff Ignimbrite (Pantelleria, Italy). Journal of Petrology 59, 2245–2272. https://doi.org/10.1093/petrology/egy095

Lowenstern, J. B., 1994. Chlorine, fluid immiscibility, and degassing in peralkaline magmas from Pantelleria, Italy. American Mineralogist 79, 353-369.

Macdonald, R., 1974. Nomenclature and petrochemistry of the peralkaline oversaturated extrusive rocks. Bulletin of Volcanology. 38, 498–516. https://doi.org/10.1007/BF02596896

Macdonald, R., 2012. Evolution of peralkaline silicic complexes: Lessons from the extrusive rocks. Lithos 152, 11–22. https://doi.org/10.1016/j.lithos.2012.01.014

Macdonald, R., Belkin, H. E., Fitton, J. G., Rogers, N. W., Nejbert, K., Tindle, A. G., Marshall, A. S., 2008. The Roles of Fractional Crystallization, Magma Mixing, Crystal Mush Remobilization and Volatile-Melt Interactions in the Genesis of a Young Basalt-Peralkaline Rhyolite Suite, the Greater Olkaria Volcanic Complex, Kenya Rift Valley. Journal of Petrology 49(8), 1515-1547, DOI: 10.1093/petrology/egn036

Macdonald, R., Bagiński, B., Leat, P.T., White, J.C., Dzierżanowski, P., 2011. Mineral stability in peralkaline silicic rocks: Information from trachytes of the Menengai volcano, Kenya. Lithos 125, 553–568. https://doi.org/10.1016/j.lithos.2011.03.011

Macdonald, R., Bagiński, B., Ronga, F., Dzierżanowski, P., Lustrino, M., Marzoli, A., Melluso, L., 2012. Evidence for extreme fractionation of peralkaline silicic magmas, the Boseti volcanic complex, Main Ethiopian Rift. Mineralogy and Petrology. 104, 163–175. https://doi.org/10.1007/s00710-011-0184-4

Macdonald, R., Bagiński, B., Belkin, H., White, J.C., Noble, D.C., 2019. The Gold Flat Tuff, Nevada: Insights into the evolution of peralkaline silicic magmas. Lithos 328–329. https://doi.org/10.1016/j.lithos.2019.01.017

Mahood, G.A., 1984. Pyroclastic rocks and calderas associated with strongly peralkaline magmatism. Journal of Geophysical Research. 89, 8540. https://doi.org/10.1029/JB089iB10p08540

Mahood, G.A., Hildreth, W., 1986. Geology of the peralkaline volcano at Pantelleria, Strait of Sicily. Bulletin of Volcanology. 48, 143–172. https://doi.org/10.1007/BF01046548

Mahood, G.A., Stimac, J.A., 1990. Trace-element partitioning in pantellerites and trachytes. Geochimica et Cosmochimica Acta 54, 2257–2276. https://doi.org/10.1016/0016-7037(90)90050-U

Manning, D.A.C., 1981. The effect of fluorine on liquidus phase relationships in the system Qz-Ab-Or with excess water at 1 kb. Contributions to Mineralogy and Petrology. 76, 206–215. https://doi.org/10.1007/BF00371960

Markl, G., Marks, M.A., Frost, B.R., 2010. On the controls of oxygen fugacity in the generation and

crystallization of peralkaline melts. Journal of Petrology 51, 1831-1847. https://doi.10.1093/petrology/egq040.

Marks, M., 2003. Quantification of Magmatic and Hydrothermal Processes in a Peralkaline Syenite-Alkali Granite Complex Based on Textures, Phase Equilibria, and Stable and Radiogenic Isotopes. Journal of Petrology 44, 1247–1280. https://doi.org/10.1093/petrology/44.7.1247

Marsh 1975 Aenigmatite stability in silica-undersatu- rated rocks. Contrib. Mineralogy and Petrology. 50, 135-144.

Marshall, A.S., Macdonald, R., Rogers, N.W., Fitton, J.G., Tindle, A.G., Nejbert, K., Hinton, R.W., 2009. Fractionation of Peralkaline Silicic Magmas: the Greater Olkaria Volcanic Complex, Kenya Rift Valley. Journal of Petrology 50, 323–359. https://doi.org/10.1093/petrology/egp001

Morimoto, N. and Kitamura, M., 1983. Q-J diagram for classification of pyroxenes. J. Jap Assoc Mineral Petrol Econ Geol 78: 141.

Neave, D.A., Fabbro, G., Herd, R.A., Petrone, C.M., Edmonds, M., 2012. Melting, Differentiation and Degassing at the Pantelleria Volcano, Italy. Journal of Petrology 53, 637–663. https://doi.org/10.1093/petrology/egr074

Nicholls, J., Carmichael, J.S.E., 1969a. Peralkaline acid liquids: A petrological study. Contributions to Mineralogy and Petrology. 20, 268–294. https://doi.org/10.1007/BF00377480

O'Neill, H.S.C., Pownceby, M.I., 1993. Thermodynamic data from redox reactions at high temperatures. I. An experimental and theoretical assessment of the electrochemical method using stabilized zirconia eletrolytes, with revised values for the Fe-"FeO", Co-CoO, Ni-NiO and Cu-Cu_2O oxygen buffers, and new data for the W-WO_2 buffer. Contributions to Mineralogy and Petrology 114, 296–314. https://doi.org/10.1007/BF01046533.

Pownceby, M.I., O'Neill, H.S.C., 1994. Thermodynamic data from redox reactions at high temperatures. III. Activity-composition relations in Ni-Pd alloys from EMF measurements at 850–1250 K, and calibration of the NiO+Ni-Pd assemblage as a redox sensor. Contributions to Mineralogy and Petrology. 116, 327–339. https://doi.org/10.1007/BF00306501

Ren, M., Omenda, P., Anthony, E., White, J., Macdonald, R., Bailey, D., 2006. Application of the QUILF thermobarometer to the peralkaline trachytes and pantellerites of the Eburru volcanic complex, East African Rift, Kenya. Lithos 91, 109–124. https://doi.org/10.1016/j.lithos.2006.03.011

Robie, R.A., Hemingway, B.S., 1995. Thermodynamic properties of minerals and related substances at 298.15K and 1 bar (10^5 pascals) pressure and at higher temperatures. U.S. Geological Survey Bulletin 2131.

Roeder, P. L., & Emslie, R., 1970. Olivine-liquid equilibrium. Contributions to mineralogy and petrology, 29(4), 275-289.

Romano, P., Andújar, J., Scaillet, B., Romengo, N., Di Carlo, I., Rotolo, S.G., 2018. Phase Equilibria of Pantelleria Trachytes (Italy): Constraints on Pre-eruptive Conditions and on the Metaluminous to Peralkaline Transition in Silicic Magmas. Journal of Petrology 59, 559–588. https://doi.org/10.1093/petrology/egy037

Romano, P., White, J.C., Ciulla, A., Di Carlo, I., D'Oriano, C., Landi, P., Rotolo, S.G., 2019. Volatiles and trace elements content in melt inclusions from the zoned Green Tuff ignimbrite

(Pantelleria, Sicily): petrological inferences. Annals of Geophysics 62 - 1, doi: 10.4401/ag-7671

Rotolo, S.G., La Felice, S., Mangalaviti, A., Landi, P., 2007. Geology and petrochemistry of the recent (<25 ka) silicic volcanism at Pantelleria Island. Bollettino della Società Geologica Italiana 126, 191–208.

Rotolo, S.G., Scaillet, S., La Felice, S., Vita-Scaillet, G., 2013. A revision of the structure and stratigraphy of pre-Green Tuff ignimbrites at Pantelleria (Strait of Sicily). Journal of Volcanology and Geothermal Research 250, 61–74. https://doi.org/10.1016/j.jvolgeores.2012.10.009.

Roux, J., & Lefevre, A., 1992. A fast-quench device for internally heated pressure vessels. European journal of mineralogy, 279-282.

Scaillet, B., Pichavant, M., Roux, J., Humbert, G., Lefevre, A., 1992. Improvements of the Shaw membrane technique for measurement and control of fH_2 at high temperatures and pressures. American Mineralogist. 77, 647–655.

Scaillet, B., Pichavant, M., Roux, J., 1995. Experimental Crystallization of Leucogranite Magmas. Journal of Petrology 36, 663–705.

Scaillet, B., Macdonald, R., 2001. Phase Relations of Peralkaline Silicic Magmas and Petrogenetic Implications. Journal of Petrology 42, 825–845. https://doi.org/10.1093/petrology/42.4.825.

Scaillet, B., Macdonald, R., 2003a. Experimental Constraints on the Relationships between Peralkaline Rhyolites of the Kenya Rift Valley. Journal of Petrology 44, 1867–1894. https://doi.org/10.1093/petrology/egg062

Scaillet, B., Macdonald, R., 2006. Experimental constraints on pre-eruption conditions of pantelleritic magmas: Evidence from the Eburru complex, Kenya Rift. Lithos 91, 95–108. https://doi.org/10.1016/j.lithos.2006.03.010

Scaillet, B., Pichavant, M., Cioni, R., 2008. Upward migration of Vesuvius magma chamber over the past 20,000 years. Nature 455, 216–219. https://doi.org/10.1038/nature07232

Scaillet, B., Holtz, F., Pichavant, M., 2016. Experimental Constraints on the Formation of Silicic Magmas. Elements 12, 109-114.

Scaillet, S., Rotolo, S.G., La Felice, S., Vita-Scaillet, G., 2011. High-resolution 40Ar/39Ar chronostratigraphy of the post-caldera (<20ka) volcanic activity at Pantelleria, Sicily Strait. Earth and Planetary Science Letters 309, 280–290. https://doi.org/10.1016/j.epsl.2011.07.009

Scaillet, S., Vita-Scaillet, G., Rotolo, S.G., 2013. Millenial-scale phase relationships between ice-core and Mediterranean marine records: insights from high-precision 40Ar/39Ar dating of the Green Tuff of Pantelleria, Sicily Strait. Quaternary Science Reviews 78, 141-154

Sisson, T. W., & Grove, T. L. (1993). Experimental investigations of the role of H_2O in calc-alkaline differentiation and subduction zone magmatism. Contributions to Mineralogy and Petrology, *113*(2), 143-166.

Taylor, J.R., Wall, V.J., Pownceby, M.I., 1992. The calibration and application of accurate redox sensors. American Mineralogist. 77, 284–295.

Toplis, M. J., 2005. The thermodynamics of iron and magnesium partitioning between olivine and

liquid: criteria for assessing and predicting equilibrium in natural and experimental systems. Contributions to Mineralogy and Petrology, 149(1), 22-39.

White, J.C., 2011. A method for estimating temperature and oxygen fugacity for an assemblage of clinopyroxene, aenigmatite, ilmenite, and quartz in peralkalic rhyolite. Geological Society of America Abstracts with Programs 43(5), 90.

White, J.C., Ren, M., Parker, D.F., 2005. Variation in mineralogy, temperature, and oxygen fugacity in a suite of strongly peralkaline lavas and tuffs, pantelleria, Italy. Canadian Mineralogist 43, 1331–1347. https://doi.org/10.2113/gscanmin.43.4.1331

White, J.C., Parker, D.F., Ren, M., 2009. The origin of trachyte and pantellerite from Pantelleria, Italy: Insights from major element, trace element, and thermodynamic modelling. Journal of Volcanology and Geothermal Research 179, 33–55. https://doi.org/10.1016/j.jvolgeores.2008.10.007

Williams, R., Branney, M.J., Barry, T.L., 2014. Temporal and spatial evolution of a waxing then waning catastrophic density current revealed by chemical mapping. Geology 42, 107–110. https://doi.org/10.1130/G34830.1

Fig. 1: (a) General tectonic sketch of Sicily Channel Rift Zone showing the location of Pantelleria in the rift zone between Sicily and Tunisia. (b) Simplified geological map of Pantelleria Island.

Fig. 2: Variation of (a) melt and (b) alkali feldspar proportions versus melt water content (H_2O_{melt}). (c) Variation of crystal content, alkali feldspar content and the sum of mafic minerals (clinopyroxene+olivine+aenigmatite+amphibole) as a function of melt proportion. Opens symbols are for Fastuca (FTP) whereas filled symbols are for Green Tuff (GTP).

Fig. 3: Phase relationship at 1.0 kbar in the T-H_2Omelt space for the (a) Green Tuff pantellerite (GTP) (ΔNNO -0.41 to -2.54) and (b) Fastuca pantellerite (FTP) (ΔNNO -1.25 to -2.45), countoured/colored for iso-log fO$_2$ lines. (c) For comparison, the phase diagram established by Di Carlo et al. (2010) (ΔNNO -1.37 to -2.9) on Fastuca pantellerite is also shown. Cpx, clinopyroxene; Ol, olivine; Afs, alkali feldspar; Qz; quartz; Ilm; ilmenite; Aenig, aenigmatite; Amph, amphibole.

Fig. 4: Composition of experimental clinopyroxene. (a) Classification of experimental clinopyroxene (Morimoto and Kitamura, 1983) Q = Ca+Mg+Fe^{2+} and J= 2Na. (b) Variation of total iron content (expressed as XFe= Fe$_{tot}$ /(Fe$_{tot}$+Mg)) vs melt water content. (c) Variation of XFe with oxygen fugacity (expressed as ΔNNO). (d) Variation of Na$_2$O content in clinopyroxene with melt peralkalinity index. The grey box represents the composition of natural clinopyroxene in Fastuca pantellerite, whereas the white box that of the Green Tuff pantellerite.

Fig. 5: Composition of experimental olivine. Variation of fayalite content with (a) oxygen fugacity (expressed as ΔNNO) and (b) melt water content. The grey box indicates the olivine composition in pantellerite rocks. (c) Ternary diagram for olivine classification (mol %, Fo, forsterite; Fa, fayalite; Tephr, tephroite), in which are plotted the compositions of experimental olivine synthetized in trachytes (black dots) by Romano et al. (2018) and the composition of natural olivines in trachyte and pantellerite (grey crosses).

Fig. 6: Variation of XTi [=Ti/(Ti+Fe)] of experimental aenigmatite with temperature. Open symbols are Fastuca pantellerite (FTP) whereas filled symbols are for Green Tuff pantellerite (GTP). Grey crosses are the experimental aenigmatite of Di Carlo et al. (2010) and the grey box represents the composition of natural aenigmatites of Pantelleria.

Fig. 7: Composition of experimental amphibole. (a) Variation of XFe [=Fe/(Fe+Mg)] as a function of temperature, (b) Na_2O content vs melt water content, (c) CaO content vs melt water content. Open symbols are for Fastuca pantellerite (FTP) whereas filled symbols are for Green Tuff pantellerite (GTP). The grey box represents the composition of natural amphibole in FTP, whereas the white box that of GTP.

Fig. 8: Composition of experimental alkali feldspar. Variation of Or (mole %) content as a function of (a) melt water content and (b) temperature. The white box indicates the average composition of alkali feldspar in pantellerite rocks of Pantelleria.

Fig. 9: Composition of experimental glasses. Variation of crystal content as a function of (a) SiO_2 wt%, (b) FeO wt%, (c) Al_2O_3 wt%. The grey box indicates the average whole rock and melt inclusion compositions of pantelleritic rocks. (d), Left triangle: FeO - Al_2O_3 - Na_2O+K_2O (moles) projection showing the positions of glass FTP and coexisting mineral phases for FTP. The vertical dashed line separates peraluminous from peralkaline compositions. (d), Right triangle: selected glass compositions of FTP experiments at 750°C and 680°C with tie lines to coexisting minerals: the solid arrowed lines show the effect of alkali feldspar crystallization on melt composition, the dashed arrow that of cpx+amphibole and the point-dashed arrow that of cpx+fayalite (see also Scaillet and Macdonald, 2003).

Fig. 10: Ulvospinel (a) and Ilmenite compositions (b) plotted against the oxygen fugacity (expressed as ΔNNO) for Pantelleria and Eburru samples. Black lines correspond to the equations in paragraph *5.3.2*.

Fig. 11: Silica activity plotted against temperature for Pantelleria samples. Symbols represent the minerals assemblages in pantelleritic rocks, pressure was taken at 1.0 kbar. The solid lines are relevant to the composition of the natural (a) $Usp_{71.3}$; (b) $XIlm_{95.6}$ and $XFa_{92.1}$ (c) ΔNNO -1.66 $Ilm_{95.6}$, $XFa_{92.1}$; (d) $Ilm_{96.8}$ (ΔNNO -2.0) $Ilm_{93.8}$ (ΔNNO -0.9).

Fig. 12: Comparison of experimental and natural amphiboles taking in consideration the Na content plotted against (a) ΔNNO and (b) iron content.

Fig.13: Comparison of experimental glasses with natural whole-rock and melt inclusions in the (a) Macdonald (1974) diagram for peralkaline rocks and (b) FeO/Al_2O_3 (wt%) vs. Peralkalinity index diagram. Literature data (grey crosses), taken from White et al. 2005, Gioncada and Landi, (2010); Neave et al. (2012); Lanzo et al. (2013); Romano et al. (2019). Grey stars represent the experimental glasses of Di Carlo et al. (2010).

Table 1. Composition of the starting glasses Green Tuff Pantellerite (GTP) and Fastuca Pantellerite (FTP) and the respective natural mineral phases in the starting rocks

GTP	Starting material	Afs	sd	Cpx	sd	Ol	sd	Aenig	sd	Ilm	sd
n:	20	20		6		4		9		4	
SiO$_2$ (wt%)	72.60	67.16	0.79	49.25	0.41	30.32	0.7	41.38	0.64	0.1	0
TiO$_2$	0.52	0.03	0	0.36	0.12	0	0	8.97	0.23	49.41	0.22
Al$_2$O$_3$	9.00	17.73	0.27	0.14	0.05	0	0	0.66	0.04	0.03	0.01
FeO$_{tot}$	6.24	0.84	0.1	25.33	0.87	62.01	1.5	39.67	0.61	43.78	0.3
MnO	0.24	0	0	1.42	0.19	2	0.05	1.21	0.13	1.92	0.03
MgO	0.51	0	0	3.16	0.49	4.05	2	0.99	0.37	0.01	0
CaO	0.46	0.01	0.01	16.84	0.79	0.43	0.43	0.63	0.08	0.02	0.01
Na$_2$O	7.29	7.63	0.29	1.96	0.25	0	0	6.62	0.2	0	0
K$_2$O	2.87	6.14	0.23	0.06	0	0	0	0.03	0	0	0
P2O5	0.06	0	0	0	0	0	0	0	0	0	0
F	0.20										
sum	100	99.51	0.81	100.6	0.8	99.11	0.92	98.84	0.88	95.3	0.31
P.I	1.68										
Fa						90.41					
Wo				39.97							
En				10.44							
Fs				49.59							
An		0.1									
Ab		65.3									
Or		34.6									

FTP*	Starting material	Afs	sd	Cpx	sd	Ol	sd	Aenig	sd	Amph	sd	Na-cpx	sd
n:													
SiO$_2$ (wt%)	69.45	65		47.2		29.28		40.5		49.2		52.9	
TiO2	0.48	0		0.73		0.07		9		1.77		0.22	
Al$_2$O$_3$	10.15	18.45		0.42		0.2		0.52		0.65		0.77	
FeO$_{tot}$	7.87	1.05		27.7		65.15		40.5		34.2		32.3	
MnO	0.21	0		1.42		3.93		1.22		1.16		0.84	
MgO	0.1	0		1.33		0.9		0.4		0.89		0.08	
CaO	0.53	0		17.9		0.47		0.52		3.3		1.36	
Na$_2$O	6.71	7.42		1.77		0		7.11		7.32		11.21	
K$_2$O	4.46	6.19		0		0		0.01		1.48		0.16	
P2O5	0.04	0		0		0		0		0		0	
sum	100	98.1		98.5		100		99.8		100		99.8	
P.I	1.56												
Fa						92.1							
Wo				42.98									
En				4.44									
Fs				52.57									

An	0.01
Ab	64.56
Or	35.44

n, number of analyses; sd, standard deviation; FeOtot total iron reported as FeO. Ol, olivine; cpx, clinopyroxene; afs, alkali feldspar, mt, magnetite; ilm, ilmenite. Fa (mol%)=100(Mg/Mg+FeOtot) in olivine. Wo, En and Fs were calculated as in the study by Morimoto (1989). P.I = peralkalinity index (molar Na_2O+K_2O/Al_2O_3). An=100[Ca/(Ca+Na+K)]; Ab=100[Na/(Ca+Na+K)]; Or=100[K/(Ca+Na+K)]. End-members calculated as in the study by Deer et al. (1992).*Apart from the starting material, the analyses of mineral phases are taken from Di Carlo et al. 2010.

Table 10. Compilation of natural data for pantellerites and associated trachytes with results of QUIlF geothermometry (ol-cpx equilibrium) calculated at P = 1000 bar.

				Whole Rock Composition		Clinopyroxene			Ol	Spinel	Ilm	Aen	Amphibole		QUILF95 Results				
				wt% (normalized)															
Sample	Source	P.I.	Class	FeO*	Al$_2$O$_3$	apfu Ca	apfu Na	X-Fe(tot)	XFa	XUsp	XIlm	Ti#	X-Fe(tot)	^{VI}Na	T (°C)	a$_{SiO2}$ (Qtz)	log fO$_2$	ΔFMQ*	ΔNNO
Pantelleria, Italy																			
231	MS90	1.05	CT	5.24	15.79	0.8157	0.0276	0.4994	0.7358	0.7220					904	0.816	-13.42	-0.89	-1.55
Pan1401	R19	1.07	CT	7.06	15.66	0.8273	0.0407	0.5089	0.7461		0.9504				899	0.837	-13.67	-1.05	-1.71
150522	L18	1.01	CT	5.35	15.39	0.8235	0.0445	0.5168	0.7469		+				881	0.743			
226	MS90	1.19	C	6.40	13.18	0.8061	0.0413	0.6598	0.8591	0.7665					879	0.922	-14.23	-1.24	-1.91
98520	W05	1.27	P	6.33	12.60	0.8500	0.0559	0.8341	0.9341	0.6802	0.9465				830	0.836	-14.87	-0.93	-1.61
150541	L18	1.08	C	4.95	14.08	0.7982	0.0722	0.6937	0.8457		0.9556				804	0.904	-15.22	-0.73	-1.42
060522	W09	1.09	C	4.15	14.25	0.7872	0.0590	0.6424	0.8378	0.6419					799	0.896	-15.25	-0.66	-1.35
98526	W05	1.42	P	5.87	11.82	0.7958	0.0911	0.8013	0.9374		0.93.2				794	1.000	-15.15	-0.45	-1.14
160541	L18	1.20	P	6.47	11.54	0.8200	0.1019	0.8280	0.9208		0..556	0.17			793	0.942	-15.69	-0.97	-1.66
98531	W05	1.62	P	7.65	10.31	0.8371	0.0857	0.9031	0.9721		0.9.61	0.16			763	1.000	-15.77	-0.37	-1.07
98523	W05	1.55	P	6.38	10.44	0.7484	0.1400	0.8655	0.9408		0..17	0.15			756	1.000	-15.76	-0.20	-0.91
060537	W09	1.62	P	6.45	9.41	0.7233	0.1463	0.8334	0.9414		0.9589	0.16			744	1.000	-16.70	-0.86	-1.57
98522	W05	1.75	P	8.56	9.33	0.7276	0.2021	0.7522			0.9441	0.15			*733*	*1.000*	*-16.46*	*-0.35*	*-1.06*
98521	W05	1.75	P	8.40	9.35	0.7254	0.2107	0.8.41			0.9378	0.16			*733*	*1.000*	*-16.29*	*-0.19*	*-0.90*
98527	W05	1.61	P	7.09	8.79	0.7136	0.1829	0.8430			0.9374	0.16	0.7941	1.06	*729*	*1.000*	*-16.37*	*-0.17*	*-0.88*
150514	L18	1.39	P	7.73	9.72	0.7364	0.1725	0.84.3			0.9524	0.17			*724*	*1.000*	*-16.86*	*-0.53*	*-1.24*
060501	W09	1.82	P	6.57	9.26	0.7233	0.1463	0.8334	0.9535		0.9429	0.16	0.9201	1.23	718	1.000	-16.76	-0.28	-0.99
150546	L18	1.53	P	7.68	10.36	0.7300	0.1626	0.8349			+	0.17							
150544	L18	1.61	P	7.84	9.91	0.7301	0.1644	0.8428			+	0.17							
150521	L18	1.63	P	7.65	9.56	0.7312	0.1604	0.8442				0.17							
150511	L18	1.68	P	7.85	9.40	0.7451	0.1488	0.8504				0.18							
060545	W09	1.74	P	7.91	9.17	0.7439	0.1302	0.8430		0.7971		0.17							
98529	W05	1.97	P	8.41	7.72	0.7158	0.2032	0.9263				0.16							
Eburru, Kenya																			
2keb8	R06	1.24	P	8.35	11.40	0.8083	0.1193	0.9723	0.9917		0.9724	0.15			721	1.000	-17.79	-1.39	-2.10
keb17	R06					0.6906	0.2727	0.9839			0.9754	0.16	0.9529	1.2	*719*	*1.000*	*-17.88*	*-1.42*	*-2.13*
keb8	R06	1.24	P	8.35	11.40	0.8083	0.1193	0.9723	0.9919		0.9651	0.15			716	0.970	-17.56	-1.03	-1.74
keb13	R06	1.25	P	10.13	10.34	0.7839	0.1504	0.9634	0.9878		0.9598	0.16			715	0.948	-17.41	-0.86	-1.57
keb16	R06	1.10	CT	5.82	14.32	0.8004	0.1349	0.9847	0.9957		0.9558	0.15	0.9602	1.32	712	0.990	-17.29	-0.66	-1.37
keb6	R06	1.70	P	7.80	8.89	0.6849	0.2199	0.9790	0.9925		0.9573	0.15	0.9773	1.21	684	1.000	-17.93	-0.56	-1.29
Menengai, Kenya																			
M8	M11	1.21	CT	5.41	15.00	0.8626	0.0441	0.5520	0.7765	0.7873					867	0.706	-14.65	-1.43	-2.10
K1A34/1low	M11	1.00	CT	5.38	15.81	0.8553	0.0753	0.5692	0.7841	0.7329					806	0.636	-15.71	-1.27	-1.96
K1A34/1high	M11	1.00	CT	5.38	15.81	0.8589	0.0722	0.6633	0.7841	0.7329					798	0.610	-15.94	-1.33	-2.01

RJK6	M11	1.43	PT	6.99	13.55	0.8550	0.0464	0.6029	0.7966	0.7865		864	0.654	-14.88	-1.61	-2.28
H2	M11								0.8322	0.7580		850	0.676	-14.59	-1.05	-1.73
K1A13	M11	1.42	PT	8.57	11.96	0.8365	0.0612	0.8429	0.9679	0.7329		793	0.867	-16.01	-1.29	-1.98

Data sources: MS90, Mahood and Stimac (1990); W05, White et al. (2005); R06, Ren et al. (2006); M11, Macdonald et al. (2011); R19, Romano et al. (2019); L18, Liszewska et al. (2018). P.I., peralkalinity index [= mol Na + K / Al]; Class (Macdonald, 1974): CT, Comenditic Trachyte; C, Comendite; P, Pantellerite; apfu, atoms per formula unit; X-Fe(tot) = apfu Fe/(Fe+Mg) in clinopyroxene and Ti# = apfu Ti/(Ti+Fe) in aenigmatite, where Fe = $Fe^{2+} + Fe^{3+}$; ^{VI}Na, apfu Na in amphibole octahedral site; all classify as ferroricthterite (<1.50); +, present but not analyzed; $aSiO_2(Qz)$, silica activity relative to quartz; $\Delta FMQ = \log fO_2$ - FMQ(T, P), formula in Table 11; $\Delta NNO = \log fO_2$ - NNO(T,P), calculated following O'Neill and Powenceby (1993) with the pressure correction following Pownceby and O'Neill (1994). Reported QUILF95 temperatures are calculated from clinopyroxene-olivine equilibrium. Results in italics were calculated from cpx-ilm-aen equilibrium with QUILF following White (2011); see the text for details.

Table 11. Thermodynamic parameters of the reactions describing the relationships between the mineral phases

		$\log fO_2 = AT^{-1} + B + C(P-1)T^{-1}$	
Assemblage	Reaction	A	B	C	Citation / Notes
FMQ	$3Fa + O_2 = 2Mgt + 3Qz$	-24863	8.511	0.095	Recalculated with Robie and Hemingway (1995)
FHQ	$2Fa + O_2 = 2Hem + 2Qz$	-25545	10.869	0.069	Recalculated with Robie and Hemingway (1995)
Aen=Ilm	$Aen + O_2 = Nds + 4Qz + (2Hem + Ilm)$	-22667	8.532	-0.219	White et al. (2005); Macdonald et al. (2011)
Aen=Mgt	$2Aen + O_2 = 2Nds + 8Qz + (2Mgt + 2Usp)$	-16858	2.193	-0.447	Marsh (1975)
		$\log aSiO_2(Qz) = AT^{-1} + B + C(P-1)T^{-1}$	
QUIlF	$2Usp + Qz = 2Ilm + Fa$	-2248.0	1.644	-0.035	Recalculated with Robie and Hemingway (1995)
Ilm=Aen	$\frac{1}{4}Nds + \frac{1}{2}Hem + \frac{1}{4}Ilm + Qz = \frac{1}{4}Aen + \frac{1}{4}O_2$	5666.7	-2.133	0.055	White et al. (2005); Macdonald et al. (2011)
Mgt=Aen	$\frac{1}{4}Nds + \frac{1}{4}Hem + \frac{1}{4}Ilm + Qz = \frac{1}{4}Aen + \frac{1}{8}O_2$	2107.3	-0.274	0.056	Derived from Marsh (1975)
Ilm-Fa=Aen	$\frac{1}{2}Ilm + Fa + \frac{1}{2}Nds + Qz = \frac{1}{2}Aen$	-1439.4	1.168	0.144	Macdonald et al. (2011)
Ilm-Fa=Aen+O_2	$\frac{1}{3}Ilm + \frac{1}{3}Hem + \frac{1}{3}Fa + \frac{1}{3}Nds + Qz = \frac{1}{3}Aen + \frac{1}{6}O_2$	3298.6	-1.033	0.085	This study

Temperature (T) in K, Pressure (P) in bars. T range is 800-1200 K for all reactions. Free energy and molecular volume data for ilmenite, hematite, magnetite, magnetite, ulvöspinel, fayalite, and quartz are from Robie and Hemingway (1995), Nds (melt) from Chase et al. (1985).

Table 2. Experimental run conditions and results

Green Tuff pantellerite (GTP)

Run	XH$_2$O (in moles) [1]	H$_2$O$_{melt}$ (wt%) [2]	H$_2$O$_{melt}$ by-diff (wt%) [3]	fH$_2$ (bar) [4]	log fO$_2$ (bar) [5]	Δ NNO [6]	Phase assemblage and abundances (wt%)	Crystal (wt%)	R^2
GT-R 2, 900°C, 1000 bar, PH$_2$[7]=6 bar (target: FMQ buffer), 96h									
1	1	4.52	-	11.72	-12.35	-0.41	Gl only	-	-
2	0.81	3.1	-	11.72	-12.95	-1.02	Gl only	-	-
3	0.52	1.29	-	11.72	-14.35	-2.41	Gl only	-	-
GT-R 4, 850°C, 1000 bar, PH$_2$= 6 bar, 145h									
1	1	4.52	4.65	11.90	-13.35	-0.48	Gl only	-	-
2	0.81	4	3.6	11.90	-13.55	-0.68	Gl only	-	-
3	0.52	3.1	2.23	11.90	-13.96	-1.08	Gl only	-	-
4	0.26	2.35	2.11	11.90	-14.4	-1.53	Gl (97.0), Cpx (2.4)	2.4	1.01
5	0.1	1.29	-	11.90	15.36	2.48	Gl (96.1), Cpx (1.1), afs (2.8)	3.9	0.62
GT-R 1, 800°C, 1000 bar, PH$_2$=6 bar, 196 h									
1	1	4.52	4.25	11.44	-14.4	-0.52	Gl (97.7), Cpx (1.3), Amph (1.0)	2.3	0.28
2	0.82	4.01	3.22	11.44	-14.59	-0.7	Gl (96.1), Cpx (0.8), Amph (3.1)	3.9	0.71
3	0.51	3.1	-	11.44	-14.99	-1.11	Gl (95.0), Cpx (1.1), Amph (1.4), Afs (2.5)	5	0.4
4	0.33	2.35	-	11.44	-15.44	1.55	Gl, (89.6) Cpx(0.4), Amph (1.0), Afs (6.6), qz (2.4)	10.4	0.05
5	0.1	1.29	-	11.44	16.3	-2.51	Gl, (66.1) Cpx (4.7), Amph (7.3), Afs (18.1), qz (3.22)	33.9	0.63
GT-R 3, 750°C, 1000 bar, PH$_2$=5,5bar, 96h									
1	0.99	4.53	-	10.38	15.48	-0.48	Gl (90.2), Cpx (1.1), Amph (8.7)	9.8	0.43
2	0.8	4	-	10.38	15.68	-0.68	Gl (85.8), Cpx (1.1), Amph (8.8), Afs (3.9)	14.2	0.29
3	0.48	3.1	-	10.38	-16.08	-1.09	Gl (65.5), Cpx (1.6), Amph (6,1), Afs (26.45), aenig (0.4)	34.5	0.82
4	0.3	2.35	-	10.38	-16.53	-1.53	Gl, Cpx, Amph, Afs	-	-
5	0.1	1.3	-	10.38	-17.48	-2.54	Gl, Cpx, Amph, Afs	-	-

Fastuca Pantellerite (FTP)

Run	XH$_2$O (in moles)[1]	H$_2$O$_{melt}$ (wt%)[2]	H$_2$O$_{melt}$ by-diff (wt%)[3]	fH$_2$ (bar)[4]	log fO$_2$ (bar)[5]	Δ NNO[6]	Phase assemblage and abundances (wt%)	Crystal (wt%)	R^2
GT-R 14 800°C, 1000 bar, PH$_2$=6 bar (target: FMQ buffer),									
1	1	4.53	-	12.31	-14.45	-0.57	Gl only	-	-
2	0.8	4	-	12.31	-14.63	-0.75	Gl, cpx	-	-
3	0.51	3.1	-	12.31	-15.06	-1.17	Gl, cpx, Afs	-	-
4	0.32	2.35	-	12.31	-15.4	-1.51	Gl, cpx, Afs, qz	-	-
GT-R22 800°C, 1000 bar, 96 h, PH$_2$=9,5bar, (target: below FMQ buffer),									
1	1	4.52	4.4		-15.14	-1.25	Gl only	-	-
2	0.83	4.09	3.55		-15.33	-1.44	Gl only	-	-
3	0.6	3.1	2.03		-15.74	-1.85	Gl only	-	-
4	0.29	2.35	1.6		-16.18	-2.3	Gl only	-	-

GT-R20 750°C, 1000bar, PH$_2$=9,5bar, (target: below FMQ buffer),

1	1	4.53	-	-16.31	-1.31	Gl (96.2), cpx (1.2), Fa (2.6)	3.8	0.61
2	0.83	4	-	-16.51	-1.5	Gl (84.8), Cpx (1.7), Fa (1.6), Afs (11.7), ilm (0.2)	18.8	0.3
3	0.52	3.1	-	-16.92	-1.92	Gl (62.1), Cpx (1.3), Fa (4.4.) Aenig (6.1), Afs (25.2)	37.9	0.3
4	0.3	2.35	-	-17.36	-2.36	Gl (34.0), Cpx (1.0), Aenig (6.1) Afs (48.0), Qz (10.9)	66	0.8

GT-R23 680°C, 1000 bar, PH_2=9,5bar, 86 h, (target: below FMQ buffer),

1	1	4.53	-	-18.16	-1.41	Gl (72.1), Cpx (2.6), Amph (2.3), Aenig(5.3) Afs (17.6)	27.9	0.08
2	0.82	4.06	-	-18.35	-1.6	Gl (62.6), Cpx (3.7), Amph (0.7), Aenig(5.7) Afs (27.4)	37.4	0.3
3	0.58	3.1	-	-18.76	-2.01	Gl (38.8), Cpx (6.7), Amph (0.7), Aenig (4.92), Afs (42.7), Qz (6.2)	61.2	0.54
4	0.35	2.51	-	-19.21	-2.45	Gl, Cpx,Amph, Aenig, Afs,	-	-

[1]XH_2O_{in}, initial mole fraction of H_2O of the C-H-O fluid loaded in the capsule.

[2]H_2O_{melt} (wt%), dissolved melt water content determined following the method of Scaillet and Macdonald, (2006) and Andujar et al. (2016).

[3]H_2O_{melt} by-diff (wt%), dissolved melt water content determined with the by difference method of Devine et al. (1995)

[4]fH_2 (bar), hydrogen fugacity at experimental conditions obtained from the solid sensor or from the empirical relationship of Di Carlo et al. (2010) (see the text)

[5]fO_2, logarithm of the oxygen fugacity (bar) calculated from the experimental fH_2 obtained from the solid sensors (see the text).

[6]ΔNNO log fO_2-logfO_2 of the NNO and QFM buffer calculated at P and T respectively from Pownceby and O'Neill, (1994).

[7]PH_2, hydrogen pressure loaded in the vessel at room temperature.

Crystal content, values indicate the phase abundance in the charge (in wt %). Gl, glass; Cpx, clinopyroxene; Fa, fayalite; Aenig, aenigmatite; Afs, alkali feldspar; Ilm, ilmenite; Qz, quartz; Amph, amphibole.

R^2, value indicate the square residuals.

Table 3. Composition of experimental clinopyroxenes (wt%)

Green Tuff pantellerite (GTP)

Run	n.	SiO_2	TiO_2	Al_2O_3	FeO_{tot}	MnO	MgO	CaO	Na_2O	K2O	P_2O_5	Total	XFe
GT-R 4, 850°C, 1000 bar													
4	1	49.89	0.35	0.179	19.2	1.414	9.2	17.224	0.7	0.02	0.00	98.16	0.54
5	1	49.99	0.36	0.159	20.2	1.414	8.01	17.324	0.75	0.01	0.00	98.21	0.59
GT-R 1, 800°C, 1000 bar													
1	1	50.94	1.27	1.40	18.77	0.91	13.03	6.45	4.36	0.29	0.00	97.43	0.58
2	4	50.24	0.56	0.18	22.30	1.24	8.17	15.88	1.56	0.03	0.01	100.18	0.60
sd		0.50	0.13	0.02	1.24	0.22	0.11	1.07	0.21	0.03	0.02	0.44	0.20
3	4	50.27	0.51	0.26	23.80	1.42	7.83	13.73	1.31	0.07	0.00	99.32	0.63
sd		0.68	0.11	0.06	0.69	0.24	0.26	0.27	0.10	0.01	0.00	0.26	0.04
4	8	50.24	0.48	0.25	25.12	1.50	5.74	15.07	1.59	0.02	0.00	100.01	0.71
sd		0.77	0.16	0.13	1.60	0.20	2.48	2.11	0.36	0.01	0.00	0.84	0.10
5	2	51.19	0.61	0.28	23.62	1.68	8.20	12.91	1.28	0.20	0.00	99.81	0.61
sd		0.41	0.05	0.14	0.00	0.04	0.18	0.40	0.15	0.01	0.00	0.91	0.20
GT-R 3, 750°C, 1000 bar													
1	1	51.85	0.45	0.51	23.50	1.47	3.80	18.71	1.32	0.20	0.01	101.82	0.78
2	5	50.20	0.37	0.14	23.80	1.48	2.99	16.06	2.29	0.30	0.00	97.64	0.82
sd		1.04	0.11	0.04	1.41	0.22	0.17	0.64	0.19	0.00	0.00	0.19	0.15
3	4	49.40	0.40	0.24	24.83	1.10	3.16	17.14	2.17	0.01	0.00	98.53	0.82
sd		0.87	0.13	0.13	0.91	0.15	0.22	0.37	0.35	0.02	0.00	0.15	0.01
4	1	49.30	0.19	0.11	24.64	1.57	3.14	16.81	2.26	0.03	0.01	98.06	0.81

Fatsuca Pentellerite (FTP)

Run	n.	SiO_2	TiO_2	Al_2O_3	FeO_{tot}	MnO	MgO	CaO	Na_2O	K2O	P_2O_5	Total	XFe
GT-R 20, 750°C, 1000 bar													
1	10	49.71	0.70	0.83	26.45	1.45	1.78	15.50	2.68	0.26	0.00	99.36	0.89
sd		1.89	0.68	0.36	1.11	0.21	0.10	1.03	0.64	0.01	0.00	1.49	0.01
2	10	51.33	0.52	1.40	26.81	1.45	1.45	13.61	3.33	0.32	0.00	99.19	0.91
sd		1.92	0.11	0.71	1.29	0.14	0.25	1.05	0.59	0.20	0.00	1.58	0.01
3	5	48.54	0.75	0.57	29.48	1.46	1.37	13.50	3.07	0.25	0.00	98.38	0.92
sd		1.30	5.23	1.93	4.58	0.22	0.43	4.21	0.51	0.25	0.00	1.51	0.02
4	6	48.25	0.63	0.26	30.80	1.56	1.27	13.25	2.61	0.40	0.00	98.63	0.93
sd		0.65	0.31	0.07	1.33	0.14	0.05	0.20	0.88	0.20	0.00	0.56	0.00
GT-R 23, 680°C, 1000 bar													
1													
sd													
2	4	54.23	0.71	2.25	25.59	1.06	0.53	10.93	4.87	0.65	0.00	100.81	0.96
sd		1.98	0.07	0.69	0.98	0.29	0.09	0.94	0.10	0.20	0.00	1.63	0.00
3	5	54.48	0.59	2.06	25.34	1.05	0.48	8.67	6.83	0.80	0.00	100.30	0.97
sd													

n: number of analysis;
sd: standard deviation;
FeO_{tot}: Total Iron reported as FeO;
XFe is molar Fe/(Fe+Mg) in clinopyroxene

Table 4. Composition of experimental olivines (wt%)

Fastuca Pantellerite (FTP)

Run	n.	SiO2	TiO$_2$	Al$_2$O$_3$	FeO$_{tot}$	MnO	MgO	CaO	Na$_2$O	K$_2$O	P$_2$O5	Total	Fa mole%
GT-R 20, 750°C, 1000 bar													
1	3	29.56	0.00	0.05	63.30	4.40	1.17	0.25	0.00	0.03	0.06	98.84	90.62
sd		0.11	0.00	0.00	1.16	0.10	0.09	0.04	0.00	0.04	0.03	1.39	
2	3	29.32	0.03	0.02	62.72	3.82	1.13	0.23	0.05	0.04	0.08	97.45	91.4
sd		0.45	0.04	0.02	1.55	0.39	0.06	0.04	0.04	0.03	0.05	1.83	
3	4	29.48	0.04	0.00	64.78	3.52	0.94	0.21	0.05	0.03	0.10	99.16	93.03
sd		0.22	0.04	0.01	1.54	0.22	0.05	0.03	0.06	0.03	0.06	1.58	

n: number of analysis;
sd: standard deviation
FeOtot Total iron reported as FeO
Fa mole%: mole % of fayalite in olivine

Table 5. Composition of experimental magnetite and ilmenite

Fastuca Pantellerite (FTP)

Run	n.	SiO$_2$	TiO$_2$	Al$_2$O$_3$	FeO$_{tot}$	MnO	MgO	CaO	Na$_2$O	K$_2$O	P$_2$O$_5$	Total	% Ulv
GT-R 20, 750°C, 1000 bar													
3	2	0.58	48.13	0.08	44.91	2.10	0.12	0.02	0	0.25	0	95.90	96.3
sd		0.28	0.66	0.04	1.63	0.24	0.04	0.01	0.01	0.03	0.06	1.73	

Table 6. Composition of experimental aenigmatites

Green Tuff Pantellerite (GTP)

Run	n.	SiO_2	TiO_2	Al_2O_3	FeO_{tot}	MnO	MgO	CaO	Na_2O	K_2O	P_2O_5	Total
GT R-3, 750°C, 1000 bar												
2	3	40.71	8.80	0.54	39.01	1.20	1.17	0.53	7.03	0.03	0.01	99.02
sd		0.20	0.10	0.09	0.96	0.11	0.08	0.07	0.14	0.03	0.00	0.93
3	3	41.25	8.66	0.98	37.98	1.04	1.16	0.57	6.89	0.06	0.03	98.61
sd		0.82	0.86	0.63	1.90	0.25	0.11	0.03	0.20	0.09	0.01	1.97
4	2	40.74	8.24	0.53	38.98	1.09	0.93	0.58	6.83	0.03	0.01	97.96
sd		0.51	0.72	0.13	1.04	0.10	0.23	0.11	0.20	0.03	0.00	0.88
5	4	40.40	7.95	0.76	38.95	1.16	0.94	0.67	6.80	0.06	0.03	97.73
sd		0.41	1.00	0.09	0.35	0.28	0.24	0.28	0.69	0.05	0.01	0.52

Fastuca Pantellerite (FTP)

Run	n.	SiO_2	TiO_2	Al_2O_3	FeO_{tot}	MnO	MgO	CaO	Na_2O	K_2O	P_2O_5	Total
GT-R 20, 750°C, 1000 bar												
3	7	40.95	9.04	0.50	39.48	1.01	0.63	0.52	6.96	0.05	0.01	99.16
sd		0.79	1.39	0.12	2.99	0.31	0.14	1.80	0.98	0.04	0.04	2.23
4	7	40.43	8.73	0.47	40.72	1.07	0.59	0.45	6.78	0.06	0.02	99.32
sd		0.49	0.14	0.14	0.86	0.07	0.03	0.05	0.94	0.05	0.01	0.81
GT-R 23, 680°C, 1000 bar												
1	14	40.39	7.50	0.67	40.41	1.27	0.48	0.75	6.84	0.09	0.02	98.41
sd		0.64	0.43	0.21	1.33	0.14	0.04	0.46	0.44	0.05	0.07	1.17
2	5	41.99	7.32	0.86	40.97	1.15	0.44	0.59	6.94	0.04	0.05	100.35
sd		1.14	0.83	0.32	0.59	0.19	0.04	0.31	0.07	0.02	0.01	0.36
3	3	40.78	8.63	0.40	40.14	1.60	0.22	0.21	7.05	0.08	0.03	99.15
sd		0.40	0.69	0.03	0.88	0.15	0.00	0.02	0.16	0.03	0.02	0.15

n: number of analysis;
sd: standard deviation

Table 7. Composition of experimental amphiboles

Green Tuff Pantellerite (GTP)

Run	n.	SiO_2	TiO_2	Al_2O_3	FeO_{tot}	MnO	MgO	CaO	Na_2O	K_2O	P_2O_5	Cl	F	Total
GT R 1, 800°C, 1000 bar														
1	2	51.66	1.31	1.31	18.48	0.59	12.88	6.36	4.33	0.36	0.00	0.04	1.80	99.12
sd		0.91	0.21	0.15	0.99	0.09	0.30	0.32	0.17	0.03	0	0.02	0.30	0.67
2	4	51.98	1.47	1.06	18.45	0.73	12.52	6.58	4.61	0.45	0.01	0.40	1.52	99.77
sd		0.57	0.16	0.08	1.17	0.13	0.27	0.24	0.21	0.10	0.00	0.80	0.84	0.65
3	2	51.29	1.65	1.40	20.37	0.70	11.53	5.89	4.89	0.41	0.01	0.06	2.10	100.29
sd		0.42	0.20	0.27	0.82	0.20	0.54	0.39	0.16	0.09	0.00	0.02	0.18	0.75
4	3	51.73	2.07	1.23	19.14	0.61	11.79	5.95	5.26	0.46	0.03	0.04	2.41	100.71
sd		0.70	0.20	0.24	1.64	0.05	0.66	0.44	0.13	0.05	0.00	0.01	0.30	0.71
5	4	51.37	2.20	1.12	21.30	0.57	10.69	5.27	5.37	0.51	0.04	0.07	2.40	100.86
sd		1.06	0.22	0.14	1.07	0.10	0.49	0.29	0.15	0.14	0.01	0.02	0.25	1.04
GT R 3, 750°C, 1000 bar														
1	3	50.88	1.64	1.47	24.01	1.00	8.01	5.53	5.01	0.52	0.08	0.06	1.27	99.28
sd		1.84	0.27	0.67	1.53	0.15	0.81	0.50	0.33	0.09	0.02	0.04	0.20	1.61
2	4	50.31	2.03	1.38	26.47	0.87	6.00	4.74	5.15	0.57	0.05	0.067	1.029	97.52
sd		1.00	0.16	0.17	0.08	0.26	0.23	0.35	0.19	0.10	0.00	0.01	0.13	1.70
3	2	51.03	2.02	1.51	27.59	1.09	4.66	3.56	6.20	0.82	0.05	0.08	1.59	100.39
sd														
4	3	49.52	2.14	0.87	28.12	1.21	3.92	3.89	6.08	0.76	0.00	0.07	1.44	98.01
sd		0.45	0.07	0.26	0.25	0.22	0.36	0.36	0.20	0.15	0.00	0.01	0.13	0.61

Fastuca Pantellerite (FTP)

Run	n.	SiO_2	TiO_2	Al_2O_3	FeO_{tot}	MnO	MgO	CaO	Na_2O	K_2O	P_2O_5	Cl	F	Total
GT R 23, 680°C, 1000 bar														
1	4	47.44	1.56	0.96	33.47	1.30	1.60	3.94	5.69	1.03	0.02	0.03	0.78	97.83
sd		0.71	0.27	0.12	0.51	0.10	0.10	0.31	0.28	0.11	0.05	0.02	0.14	0.74
2	4	47.85	1.63	0.87	33.25	1.29	1.54	2.96	6.33	0.93	0.01	0.04	0.86	97.57
sd		0.37	0.24	0.13	0.53	0.17	0.36	0.15	0.12	0.04	0.02	0.01	0.13	0.38
3	3	48.39	2.08	0.59	33.36	1.32	0.78	2.05	6.96	1.25	0.02	0.04	0.80	97.64
sd		0.23	0.46	0.11	0.80	0.07	0.40	0.48	0.20	0.15	0.01	0.01	0.29	0.49

n: number of analysis;
sd: standard deviation

Table 8. Composition of experimental alkali feldspars (wt%)

Green Tuff Pantellerite (GTP)

Run	n.	SiO_2	TiO_2	Al_2O_3	FeO_{tot}	MnO	MgO	CaO	Na_2O	K_2O	P_2O_5	Total	An-Or (%)
GT-R 4, 850°C, 1000 bar													
2	4	64.87	0.01	17.79	3.77	0.02	0.03	0.72	6.98	4.59	0.00	98.72	68.92 - 31.06
sd		2.09	0.02	0.54	1.38	0.03	0.04	0.43	0.85	0.53	0.00	1.12	
GT-R 1, 800°C, 1000 bar													
3	8	68.10	0.03	18.17	1.08	0.03	0.01	0.01	7.35	5.62	0.03	100.35	66.49 - 33.46
sd		0.61	0.04	0.21	0.25	0.04	0.01	0.02	0.48	0.72	0.04	0.76	
4	5	68.28	0.06	17.85	1.38	0.02	0.02	0.02	7.28	5.32	0.02	100.14	67.47 - 32.43
sd		0.71	0.07	0.68	0.49	0.02	0.03	0.03	0.47	1.77	0.02	0.86	
5	4	68.10	0.03	18.19	1.15	0.00	0.00	0.01	7.53	5.52	0.01	100.51	67.47 - 32.43
sd		0.38	0.04	0.28	0.29	0.00	0.01	0.01	0.65	0.95	0.02	0.27	
GT-R 3, 750°C, 1000 bar													
2	4	67.74	0.02	17.71	1.09	0.01	0.00	0.00	7.34	6.21	0.00	100.10	64.22 - 35.75
sd		0.39	0.02	0.22	0.15	0.02	0.00	0.01	0.15	0.15	0.00	0.64	
3	3	67.92	0.04	17.81	1.09	0.02	0.01	0.06	8.17	5.04	0.02	100.08	70.96 - 28.77
sd		0.55	0.02	0.36	0.23	0.03	0.01	0.10	1.08	1.19	0.00	0.70	
4	3	67.41	0.02	17.97	0.95	0.06	0.10	0.02	7.32	4.85	0.00	98.53	64.81 - 30.30
sd		0.78	0.04	0.13	0.22	0.08	0.19	0.02	0.23	0.08	0.01	0.45	

Fastuca Pantellerite (FTP)

Run	n.	SiO_2	TiO_2	Al_2O_3	FeO_{tot}	MnO	MgO	CaO	Na_2O	K_2O	P_2O_5	Total	An-Or (%)
GT-R 20, 750°C, 1000 bar													
2	4	66.38	0.00	17.54	1.16	0.05	0.01	0.02	7.05	6.90	0.01	99.12	60.77-39.15
sd		0.60		0.19	0.19	0.06	0.02	0.02	0.20	0.28	0.03	1.01	
3	4	67.23	0.14	17.26	1.59	0.08	0.02	0.06	7.73	5.90	0.02	100.02	66.38-33.35
sd		0.66	0.01	0.23	0.28	0.02	0.03	0.10	0.43	0.26	0.01	0.92	
4	3	65.28	0.05	15.55	3.15	0.03	0.06	0.27	8.01	5.55	0.05	97.79	68.38-31.18
sd													
GT-R 23, 680°C, 1000 bar													
1	4	66.42	0.08	17.54	1.66	0.00	0.06	0.06	6.11	8.18	0.05	100.16	53.01 - 46.71
sd		0.39	0.30	0.15	0.25	0.01	0.03	0.07	0.52	0.49	0.30	0.63	
2	4	67.50	0.08	17.30	1.85	0.01	0.00	0.00	6.65	7.24	0.07	100.71	58.26 - 41.74
sd		0.47	0.30	0.28	0.43	0.08	0.01	0.00	0.22	0.24	0.20	0.60	
3	1	66.48	0.05	14.78	4.24	0.06	0.09	0.28	6.97	5.60	0.01	98.57	64.48 - 34.07
sd		1.04		0.60	0.96	0.10	0.20	0.20	1.08	0.07	0.02	0.30	

n: number of analysis;
sd: standard deviation;
FeOtot Total Iron reported as FeO;
An-Or (%): mole % of anorthite and orthoclase of the alkali feldspar.

Table 9. Composition of experimental glasses (wt%)

Green Tuff Pantellerite (GTP)

Run	n.	SiO$_2$	TiO$_2$	Al$_2$O$_3$	FeO$_{tot}$	MnO	MgO	CaO	Na$_2$O	K$_2$O	P$_2$O$_5$	Cl	F	Total
GT R2, 900°C, 1000 bar														
5	4	72.11	0.51	8.94	5.95	0.19	0.50	0.51	7.49	2.67	0.06	0.93	0.15	100.00
sd		0.21	0.04	0.07	0.30	0.02	0.44	0.24	0.29	0.31	0.01	0.04	0.13	0.00
6	3	72.83	0.53	8.97	5.28	0.29	0.53	0.44	7.20	2.88	0.07	0.87	0.12	100.00
sd		0.11	0.02	0.08	0.50	0.02	0.24	0.15	0.18	0.21	0.01	0.04	0.13	0.00
7	3	72.77	0.53	9.09	5.04	0.25	0.50	0.44	7.19	3.05	0.06	0.88	0.19	100.00
sd		0.16	0.05	0.09	0.30	0.03	0.14	0.17	0.25	0.34	0.01	0.04	0.13	0.00
GT R4, 850°C, 1000 bar														
1	4	71.02	0.48	8.91	6.48	0.29	0.55	0.80	7.21	2.93	0.01	1.12	0.19	100.00
sd		0.99	0.08	0.14	0.39	0.12	0.06	0.66	0.57	0.32	0.04	0.25	0.13	0.00
2	4	72.82	0.50	9.18	6.27	0.21	0.38	0.47	7.33	2.80	0.02	n.d	n.d	100.00
sd		0.23	0.07	0.12	0.28	0.11	0.03	0.08	0.29	0.09	0.03	n.d	n.d	0.00
3	3	72.63	0.51	9.08	5.65	0.21	0.74	0.45	7.61	3.12	0.01	n.d	n.d	100.00
sd		0.45	0.08	0.21	0.31	0.12	0.41	0.07	0.48	0.24	0.02	n.d	n.d	0.00
4	3	72.41	0.47	9.01	5.29	0.16	0.62	0.54	7.42	3.03	0.01	0.91	0.15	100.00
sd		0.31	0.08	0.10	0.40	0.04	0.24	0.34	0.19	0.11	0.01	0.04	0.13	0.00
5	3	72.76	0.52	9.05	5.36	0.07	0.53	0.52	6.98	3.12	0.00	0.90	0.26	100.00
sd		1.56	0.06	0.55	0.43	0.14	0.08	0.69	1.97	0.64	0.01	0.07	0.14	0.00
GT R1, 800°C, 1000 bar														
1	3	72.82	0.58	9.32	5.17	0.22	0.29	0.34	7.18	2.90	0.00	0.90	0.28	100.00
sd		0.23	0.06	0.10	0.22	0.06	0.03	0.05	0.18	0.12	0.05	0.12	0.03	0.00
2	4	73.00	0.48	9.42	5.57	0.24	0.29	0.33	6.67	2.91	0.02	0.89	0.18	100.00
sd		0.24	0.08	0.07	0.40	0.07	0.03	0.03	1.42	0.05	0.03	0.15	0.08	0.00
3	3	72.58	0.45	9.17	6.11	0.26	0.27	0.29	6.72	3.10	0.00	0.93	0.13	100.00
sd		0.47	0.08	0.02	0.14	0.05	0.02	0.02	0.87	0.23	0.01	0.24	0.08	0.00
4	3	72.50	0.55	8.55	6.35	0.16	0.27	0.29	7.31	2.86	0.03	0.98	0.14	100.00
sd		0.14	0.03	0.22	0.33	0.08	0.02	0.02	1.31	0.10	0.02	0.22	0.03	0.00
5	1	73.31	0.47	7.70	8.03	0.34	0.29	0.30	6.66	2.90	0.00	n.d	n.d	100.00
sd														
GT R3, 750°C, 1000 bar														
1	3	74.66	0.24	9.87	4.94	0.19	0.11	0.14	6.94	2.87	0.04			100.00
sd		0.03	0.08	0.13	0.23	0.09	0.05	0.02	0.20	0.02	0.05			0.00
2	2	74.80	0.27	9.13	5.00	0.17	0.12	0.27	6.67	3.22	0.04			100.00
sd		0.29	0.04	0.23	0.46	0.15	0.06	0.13	0.17	0.07	0.09			0.00
3	1	72.77	0.21	7.24	8.27	0.48	0.18	0.26	6.72	3.74	0.12			100.00
sd														

Fastuca Pantellerite (FTP)

Run	n.	SiO$_2$	TiO$_2$	Al$_2$O$_3$	FeO$_{tot}$	MnO	MgO	CaO	Na$_2$O	K$_2$O	P$_2$O$_5$	Cl	F	Total
GT T22, 800°C, 1000 bar														
1	5	71.59	0.47	9.69	6.77	0.31	0.08	0.56	6.05	4.44	0.04			100.00
sd		1.35	0.06	0.20	0.53	0.11	0.02	0.04	1.47	0.44	0.04			0.00

	n													
2	5	71.86	0.48	9.77	6.20	0.27	0.09	0.56	6.25	4.49	0.02			100.00
sd		0.37	0.07	0.15	0.26	0.11	0.02	0.03	0.25	0.11	0.04			0.00
3	5	71.44	0.47	9.75	6.10	0.28	0.08	0.54	6.75	4.56	0.03			100.00
sd		0.97	0.08	0.27	0.54	0.08	0.02	0.03	0.75	0.18	0.03			0.00
4	5	71.04	0.48	9.79	6.00	0.26	0.09	0.56	7.21	4.54	0.03			100.00
sd		0.42	0.07	0.17	0.44	0.10	0.02	0.05	0.30	0.15	0.04			0.00
GT T20, 750°C, 1000 bar														
1	3	71.17	0.41	9.90	6.22	0.23	0.08	0.24	6.72	4.54	0.00	0.43	0.06	100.00
sd		1.56	0.07	0.10	1.24	0.07	0.03	0.10	0.71	0.24	0.06	0.04	0.07	0.00
2	4	71.11	0.33	9.37	7.15	0.21	0.05	0.26	6.28	4.47	0.09	0.53	0.16	100.00
sd		0.44	0.05	0.13	0.19	0.09	0.02	0.02	0.38	0.14	0.05	0.03	0.10	0.00
3	3	71.06	0.52	7.54	8.28	0.43	0.06	0.31	6.97	4.11	0.00	0.52	0.20	100.00
sd		0.43	0.08	0.18	0.39	0.13	0.03	0.03	0.3?	0.20	0.00	0.05	0.08	0.00
4	3	70.93	0.55	6.42	9.09	0.63	0.07	0.44	6.??	4.20	0.01	0.54	0.25	100.00
sd		0.97	0.10	0.12	0.48	0.12	0.02	0.04	1.?4	0.20	0.03	0.03	0.07	0.00
GT T23,680°C, 1000 bar														
1	4	73.48	0.12	9.41	5.35	0.22	0.02	0.0?	6.72	4.20	0.04	0.20	0.15	100.00
sd		0.64	0.09	0.07	0.33	0.11	0.01	?.0?	0.44	0.14	0.05	0.08	0.15	0.00
2	4	73.85	0.24	8.15	6.02	0.27	0.02	0.?7	6.39	4.60	0.00	0.14	0.15	100.00
sd		0.46	0.08	0.07	0.34	0.18	0.00	0.04	0.50	0.20	0.01	0.07	0.10	0.00
3	1	73.44	0.22	6.38	8.01	0.26	0.??	0.17	6.59	4.87	0.04			100.00
sd														

n: number of analysis
sd: standard deviation

Highlights:

• Redox conditions influence liquidus and solidus temperatures of pantelleritic magmas

• Fayalitic olivine has been synthetized for first time in pantelleritic magmas

• Pantelleritic magmas evolve at temperature ≤ 750°C

•Temperature, aSiO$_2$ and fO$_2$ control mineral assemblage in peralkaline oversaturated magmas